



Review

# Comprehensive Review on g-C<sub>3</sub>N<sub>4</sub>-Based Photocatalysts for the Photocatalytic Hydrogen Production under Visible Light

Angelina V. Zhurenok <sup>1</sup>, Danila B. Vasilchenko <sup>1,2</sup> and Ekaterina A. Kozlova <sup>1,\*</sup>

<sup>1</sup> Federal Research Center Boreskov Institute of Catalysis, Siberian Branch of the Russian Academy of Science, Pr. Ak. Lavrentieva, 5, Novosibirsk 630090, Russia

<sup>2</sup> Nikolaev Institute of Inorganic Chemistry, Siberian Branch of the Russian Academy of Science, Novosibirsk 630090, Russia

\* kozlova@catalysis.ru

**Abstract:** Currently, the synthesis of active photocatalysts for the evolution of hydrogen, including photocatalysts based on graphite-like carbon nitride, is an acute issue. In this review, a comprehensive analysis of the state-of-the-art studies of graphitic carbon nitride as a photocatalyst for hydrogen production under visible light is presented. In this review, various approaches to the synthesis of photocatalysts based on g-C<sub>3</sub>N<sub>4</sub> reported in the literature were considered, including various methods for modifying and improving the structural and photocatalytic properties of this material. A thorough analysis of the literature has shown that the most commonly used methods for improving g-C<sub>3</sub>N<sub>4</sub> properties are alterations of textural characteristics by introducing templates, pore formers or pre-treatment method, doping with heteroatoms, modification with metals, and the creation of composite photocatalysts. Next, the authors considered their own detailed study on the synthesis of graphitic carbon nitride with different pre-treatments and respective photocatalysts that demonstrate high efficiency and stability in photocatalytic production of hydrogen. Particular attention was paid to describing the effect of the state of the platinum cocatalyst on the activity of the resulting photocatalyst. The decisive factors leading to the creation of active materials were discussed.

**Keywords:** g-C<sub>3</sub>N<sub>4</sub>; hydrogen; photocatalysis; platinum



**Citation:** Zhurenok, A.V.; Vasilchenko, D.B.; Kozlova, E.A. Comprehensive Review on g-C<sub>3</sub>N<sub>4</sub>-Based Photocatalysts for the Photocatalytic Hydrogen Production under Visible Light. *Int. J. Mol. Sci.* **2023**, *24*, 346. <https://doi.org/10.3390/ijms24010346>

Academic Editor: Pavel A. Abramov

Received: 10 December 2022

Revised: 21 December 2022

Accepted: 22 December 2022

Published: 25 December 2022



**Copyright:** © 2022 by the authors. Licensee MDPI, Basel, Switzerland. This article is an open access article distributed under the terms and conditions of the Creative Commons Attribution (CC BY) license (<https://creativecommons.org/licenses/by/4.0/>).

## 1. Introduction

Fossil fuels are a limited and exhaustible resource for conventional energy production that induces reasonable concerns of energy and economic crises [1]. Besides, wide use of fossil fuels causes environmental and human health impacts [2]. In this context, triggering hydrogen as an alternative energy source is a promising trend, since hydrogen is an environmentally benign fuel [3–5]. Currently, numerous industrial processes to produce hydrogen are available, but they all are energy intensive, require high temperatures, and appear economically efficient only at large scales [6]. In this regard, the photocatalytic production of hydrogen attracts particular interest as the process proceeding at ambient conditions and simulating photosynthesis, i.e., the direct conversion of solar energy into the energy of chemical bonds [7–16].

The process of photocatalytic splitting of water using TiO<sub>2</sub> catalysts under UV radiation was pioneered by Fujishima and Honda in 1972 [17]. Since that time, a great number of research has been performed to produce hydrogen by photocatalytic splitting of water with various semiconductor photocatalysts [18–22]. However, this process has an intrinsic problem of hydrogen-oxygen recombination [23]. To improve the process' quantum efficiency, photocatalytic reduction of water is carried out with the use of electron donor agents, such as various organic and inorganic compounds capable of donating electrons and thereby reducing the recombination of electron-hole pairs on the photocatalyst surface [24–26].

Promising photocatalysts activated by UV and visible light include TiO<sub>2</sub> [27–30], ZnO [31], Fe<sub>2</sub>O<sub>3</sub> [32], CdS [33], Cd<sub>1-x</sub>Zn<sub>x</sub>S [34], Bi<sub>2</sub>WO<sub>6</sub> [35], BiVO<sub>4</sub> [36], Ta<sub>2</sub>O<sub>5</sub> [37],

Ta<sub>3</sub>N<sub>5</sub> [38], and TaON [39]. Nowadays, the research and development of high-performance semiconductor photocatalysts for solving the problems of energy shortages and environmental safety are particularly important. Recently, visible-light-activated photocatalysts have been developed, which allow efficient use of the solar spectrum containing a large fraction of visible light (about 43%) [17]. Traditional semiconductor photocatalysts, such as TiO<sub>2</sub>, have a large band gap and, therefore, are unable to absorb visible light, and can be activated only by UV light, which constitutes a small fraction of the solar radiation spectrum [40–42]. Extensive searches for reliable visible-light-activated semiconductor photocatalysts revealed the next generation photocatalyst based on a polymeric semiconductor—graphitic carbon nitride [43–46].

## 2. Graphitic Carbon Nitride as a Photocatalyst

Carbon nitride, albeit known for a long time, has been tested as a photocatalyst only since 2009 [47]. Every year, the interest of researchers in this material increases, as shown in Figure 1a. It can also be seen in Figure 1b that, to date, about 10–12% of all studies on the photocatalytic H<sub>2</sub> production devoted to the synthesis and study of photocatalysts based on g-C<sub>3</sub>N<sub>4</sub> and their applications.

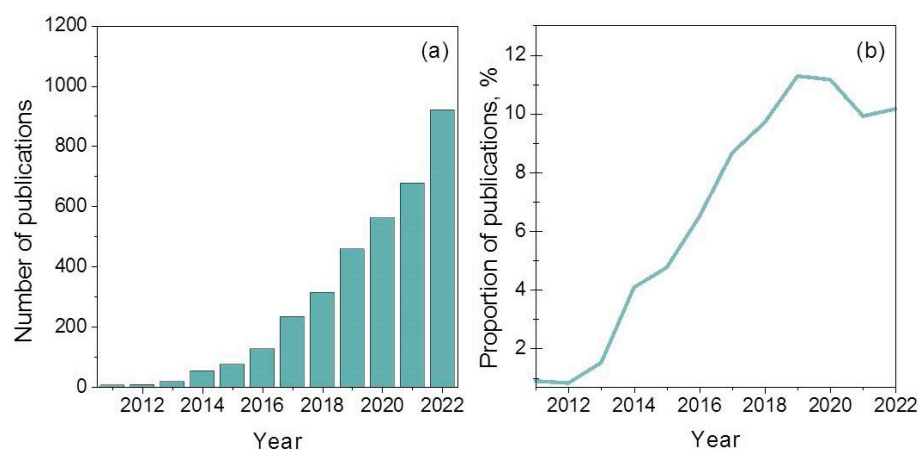


**Figure 1.** (a) Number of annual publications using “g-C<sub>3</sub>N<sub>4</sub> photocatalytic H<sub>2</sub> production” as a keyword since 2011. (b) Proportion between the number of publications with keywords “g-C<sub>3</sub>N<sub>4</sub> photocatalytic H<sub>2</sub> production” and “photocatalytic H<sub>2</sub> production” based on data of Science Direct (Elsevier).

It reveals various allotropic forms, such as  $\alpha$ -C<sub>3</sub>N<sub>4</sub>,  $\beta$ -C<sub>3</sub>N<sub>4</sub>, graphitic, cubic, and pseudocubic [48]. The most stable modification is a polymeric graphitic structure in which s-triazine or tri-s-triazine (s-heptazine) units are bound to each other through tertiary amines [47]. Graphitic carbon nitride g-C<sub>3</sub>N<sub>4</sub> has the band gap of 2.7 eV and the conduction band-edge potential  $-1.3$  V vs. NHE, which enables an efficient hydrogen production process [47]. This material is thermally and chemically stable, safe for the environment, acid and alkali resistant; its surface can be modified without infringing its composition and structure [49]. It is easily synthesized by thermal polycondensation of inexpensive nitrogen-containing precursors, such as dicyandiamide, cyanamide, melamine, urea, and thiourea [46,50–52]. The downside of this process is that it yields materials with low specific surface areas and high electron-hole recombination rates that provokes the loss in the catalytic activity [53]. To stabilize the photocatalytic activity of g-C<sub>3</sub>N<sub>4</sub>, the following approaches are used:

- Alteration of textural characteristics by introducing templates, pore formers, or pre-treatment method [54–66];
- Doping with heteroatoms [67–73];
- Modification with metals [74–90];
- Creation of composite photocatalysts [91–100].

The formation of graphitic carbon nitride proceeds by various routes at thermal condensation of the abovementioned precursors. At thermal pyrolysis, the cyclization of any of the above mentioned nitrogen-containing precursors yields melamine [49]. The dimerization of melamine at 350 °C yields melem and melon that transforms into polymeric  $g\text{-C}_3\text{N}_4$  at temperatures above 500 °C (Figure 2).

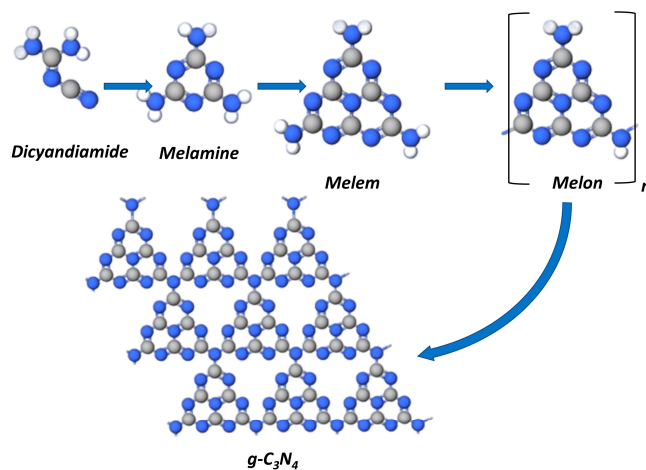


**Figure 2.** Thermal condensation of dicyandiamide to form  $g\text{-C}_3\text{N}_4$ .

Graphitic carbon nitride is known to have a defect-rich structure, which results from incomplete deamination during thermal polycondensation [49]. For this reason, synthesizing high-crystalline  $g\text{-C}_3\text{N}_4$  is a difficult task, albeit exact crystallinity (correct arrangement of atoms) is a critically important parameter affecting the band structure and charge recombination rate ( $e^-/h^+$ ) of a photocatalytically active material. A large number of structural defects increases the charge recombination rate, and thus impedes photocatalyst activity. Texture controlling can improve the chemical, physical, and optical properties of  $g\text{-C}_3\text{N}_4$  [101]. The relationship between the  $g\text{-C}_3\text{N}_4$  morphology and photocatalytic hydrogen evolution performance is discussed below.

## 2.1. Textural Characteristics and Methods to Control Them

### 2.1.1. The Use of Templates

The textural and morphological characteristics, such as porosity, specific surface area, and pore size distribution, of a carbon nitride based material can be controlled by using appropriate templates, which are subdivided into hard and soft ones. Hard templates are, for example,  $\text{SiO}_2$  and  $\text{Al}_2\text{O}_3$  [56,57]. Graphitic carbon nitrides, synthesized using these templates, possess high specific surface area and porosity, and a large number of the surface active sites. Nevertheless, soft templates, such as starch and glucose, seem much more attractive, as they are safe for the environment, require no corrosive chemicals for elimination [58,59], and provide  $g\text{-C}_3\text{N}_4$  with a specific surface area of  $>60 \text{ m}^2 \cdot \text{g}^{-1}$  [58]. After elimination of solvents and templates, the  $g\text{-C}_3\text{N}_4$  nanoporous structure turns quite delicate (fragile) and easily destroyable, which presents one of the main problems of creating polymeric hollow nanospheres. A green soft-template approach allows synthesizing various  $g\text{-C}_3\text{N}_4$  structures through relatively simple routes, keeping these structures durable even after template removal. Amphiphilic molecules, surfactants, ionic liquids, and gas bubbles are used as soft templates [60]. However, the template polymeric materials are inclined to early decomposition that results in some carbon residue in the material, which induces pores isolating, and thus affects negatively the  $g\text{-C}_3\text{N}_4$  structure and photocatalytic activity.

### 2.1.2. The Use of Pore-Forming Agents

Pore-forming agents can significantly improve the photocatalytic characteristics of graphitic carbon nitride due to their affecting of its textural characteristics. Ammonium

chloride [61] and urea [62] are among the most commonly used pore-forming agents reported in the literature. This approach ensures the synthesis of complex porous structures, such as ultrathin nanosheets [61]. Favorably compared to hard templates, the pore-forming agents require no eliminating from the target material by using harmful compounds or procedures. For example, ammonium chloride ( $\text{NH}_4\text{Cl}$ ) additive in the  $\text{g-C}_3\text{N}_4$  precursor decomposes at temperatures of 280–370 °C into  $\text{NH}_3$  and  $\text{HCl}$  thus facilitating the formation of a loose ultrathin nanosheet structure (thickness 1–2.4 nm or 3–7 atomic layers) with a defective matrix [61,63]. The bottleneck of this process is the cost-efficiency and ecological issues; obviously, the cheaper and environmentally benign pore-forming agents should be developed.

### 2.1.3. Pretreatment Method

There are many studies in which precursors are modified prior to calcination in order to obtain  $\text{g-C}_3\text{N}_4$  with improved properties [64–66]. One such modification method is the pretreatment of the precursor with acids ( $\text{H}_2\text{SO}_4$ ,  $\text{HNO}_3$ ), which makes it possible to obtain a much higher specific surface area of resulting  $\text{g-C}_3\text{N}_4$  [65]. The strong oxidizing power of the acids separates the  $\text{g-C}_3\text{N}_4$  layers into thinner nanosheets, weakening the van der Waals force between them [65]. The addition of strong alkalis ( $\text{NaOH}$ ) also facilitates the creation of ultrathin nanosheets. However, despite the ability to improve textural characteristics, it is difficult to control the yields and reproducibility of the resulting material in these pretreatment methods [65].

## 2.2. Doping Heteroatoms

The polymeric structure of graphitic carbon nitride is suitable for doping by other atoms or molecules by means of appropriate chemical procedures. The introduction of various atoms affects the electronic structure of the polymer material. Doping with nonmetals or anions leads to the  $\text{g-C}_3\text{N}_4$  band gap narrowing. It is assumed that the band gap narrowing results from the formation of localized states and elevation of the valence band maximum due to the presence of doping atoms [67]. Besides doping with mono-nonmetal heteroatoms, co-doping with several heteroatoms is applied to provide more efficient band gap width variation [68–70].

Particular attention is focused on the doping of graphitic carbon nitride with halogens: Br, I, Cl [71,72]. For example, doping with bromine increases optical absorption, conductivity, charge carrier transfer rate, and photocatalytic activity without disturbing the  $\text{g-C}_3\text{N}_4$  structural stability. It is assumed that halogen doping shifts the optical absorption spectrum towards longer wavelengths in the UV-visible spectrum [72]. The hindering of the charge carrier recombination at the introduction of Br atoms is attributed to the delocalization of the Br valence electrons to  $\pi$ -conjugated  $\text{g-C}_3\text{N}_4$  structures. Graphitic carbon nitride doped with halogen atoms (F, Cl, Br, I) exhibited enhanced optical absorption and improved photocatalytic characteristics [72]. It was found that electronegativity of the halogen atoms affects the photocatalytic properties of  $\text{g-C}_3\text{N}_4$ . The higher the halogen atomic number, the lower is its electronegativity, and more electrons can transfer from the halogen atom to  $\text{g-C}_3\text{N}_4$ , thus leading to the gradually uplifting Fermi level and decreasing work function. Doping halogen atoms facilitate the electron escape from the  $\text{g-C}_3\text{N}_4$  surface to participate in photocatalytic reactions.

Doping is an effective approach to improve the photocatalyst light absorption capacity, oxidizability, and separation efficiency of photoinduced charge carriers [73].

## 2.3. Doping Metals

One of the most frequently used and quite simple methods to modify the surface of graphitic carbon nitride is the use of metal dopants. The nanoparticles of noble and non-noble metals improve photocatalyst ability to absorb visible light and resist recombination of photoinduced charges. Also, metal nanoparticles can act as catalysts for the formation of molecular hydrogen. Noble metals attract particular attention, as they have

the most suitable electronic and optical characteristics [74,75]. The Schottky barrier, also known as the space charge separation region, is formed at the noble metal-semiconductor heterojunction; it impedes electron migration from one material to another, and reduces the charge recombination. The creation of the Schottky barrier allows for the accumulation of additional negative charges (electrons) and positive charges (holes) in the noble metal and semiconductor, respectively. Noble metals also have the ability to absorb visible light owing to the plasmon resonance effect. There are two main approaches for depositing noble metal particles on the catalyst surface: impregnation with a precursor followed by reduction with  $\text{NaBH}_4$  [76] or another reductant [83], and photodeposition under the action of ultraviolet radiation [77,84]. There is also a possibility to attach pre-synthesized nanocrystals of desired sizes and shapes on graphitic carbon nitride nanosheets through electrostatic attraction [85]. The chlorocomplexes are common precursors for the deposition of noble metals onto a  $g\text{-C}_3\text{N}_4$  surface [86–88]: for example, hexachloroplatinic acid ( $\text{H}_2\text{PtCl}_6$ ) is usually used as the platinum precursor [78,84,89]. The photodeposition method does not use high-temperature treatments or hazardous materials. The downside of using noble metals as cocatalysts is that they are very expensive, especially in view of the high metal loading in the catalysts (1–5 wt.%) [79]. Currently, many studies are aimed at replace noble metals with non-noble ones, such as copper or nickel, which are much less expensive and are able to absorb visible light [80,81,90].

Although metal doping facilitates significant acceleration of the hydrogen production reaction, an excess of cocatalyst on the surface reduces the catalyst ability to absorb light in the visible region and acts as an electron trap [82].

#### 2.4. Development of Composite Photocatalysts

In order to provide efficient light utilization and enhanced the redox ability of a material, it is common practice to shift the energy levels of the valence and conduction bands by creating a composite of two different materials. Composite materials are used to develop photocatalysts with enhanced light absorption in the visible region, efficient charge separation retarding charge recombination, and improved redox performance. There are various composite photocatalysts differing by heterojunction types: type I [91], type II [91,92], S-scheme [93,94], Z-scheme [95–97].

The creation of effective composites between two different compounds depends on their crystal structures, electron affinities, band structures, and the strength of the interfacial interaction. The type I heterojunctions assume that the valence band (VB) of semiconductor 1 lies higher than the VB of semiconductor 2, and the conduction band (CB) lies lower; in such a system, both electrons and holes are transferred to one semiconductor, where redox reactions occur [91]. Such a transfer of photogenerated charges from one semiconductor to another does not improve the efficiency of charge separation.

In type II heterojunctions, the level of VB and CB potentials of semiconductor 1 are higher than the level of VB and CB potentials of semiconductor 2. Here, the separation of photogenerated electrons and holes occurs through double charge transfer: an electron migrates from the CB of semiconductor 1 to the CB of semiconductor 2; a hole moves from the VB of semiconductor 2 to the VB of semiconductor 1. Electrons are accumulated in the CB of semiconductor 2, while holes accumulate in the VB of semiconductor 1, which facilitates efficient charge separation and reduced recombination [91,92]. Although traditional type II heterojunctions improve charge separation, they reduce the initial redox ability of electrons and holes.

The formation of S-scheme heterojunctions facilitates efficient charge separation without affecting the intrinsic redox ability of semiconductors [93]. To achieve successful construction of the S-scheme, the position of the CB and the Fermi level of the photocatalyst on which the reduction reaction proceeds must be higher than respective characteristics of the photocatalyst which runs the oxidation process. The internal electric field caused by the band deviation due to the difference in the Fermi levels of the two semiconductors enhances the charge mobility. The synthesis of two different semiconductors for subse-

quent integration into an S-scheme is considered rather difficult [94]. To date, the S-scheme heterojunction approach is considered to be the best choice for the development of photocatalysts with high charge separation efficiency and redox ability. Compared to S-scheme, the Z-scheme heterojunction photocatalysts have higher charge separation efficiency and are easier to synthesize [97]. Electrons from the CB of semiconductor 1 migrate through electron mediators (metals) to the VB of semiconductor 2 to recombine with photoinduced holes.

In the case of type I heterojunction photocatalysts [98], the redox process occurs on one semiconductor. The type II [99] heterojunctions significantly promote the separation of photoinduced electrons and holes, but have a weak redox ability that is detrimental for the photocatalytic reaction. Currently, the S-scheme approach is the most promising with regard to efficient charge separation and redox reactions [100]. However, the creation of S-scheme heterojunction photocatalysts is a difficult task that requires the structural modification of both semiconductors.

### 3. Synthesis of Graphitic Carbon Nitride to Provide Superior Photocatalytic Activity

In this section, the authors present their study performed at the Boreskov Institute of Catalysis and Nikolaev Institute of Inorganic Chemistry, that allowed the transition from the traditional precursor calcination method to the advanced synthesis of graphitic carbon nitride with improved textural and electronic characteristics, and creating highly active low-platinum catalysts for hydrogen production, which outperform the reaction rate of other catalysts reported in the literature [76,102–104].

#### 3.1. Synthesis of Graphitic Carbon Nitride by Conventional Thermal Polycondensation

At the first step of the study, g-C<sub>3</sub>N<sub>4</sub> was prepared by the traditional thermal condensation of organic precursors—melamine and dicyandiamide. The calcination was performed at varying temperatures (450, 500, 550 or 600 °C) and times (2 or 4 h) in air. In order to prevent charge recombination and increase the catalyst activity, 1–3 wt.% platinum was loaded by impregnating g-C<sub>3</sub>N<sub>4</sub> with H<sub>2</sub>PtCl<sub>6</sub>, and then followed by reducing with a 2.5-fold excess of NaBH<sub>4</sub>. After several decantations, the obtained samples were dried at 50 °C for 4 h. The synthesized photocatalysts were characterized by XRD (Figure 3a) [76].

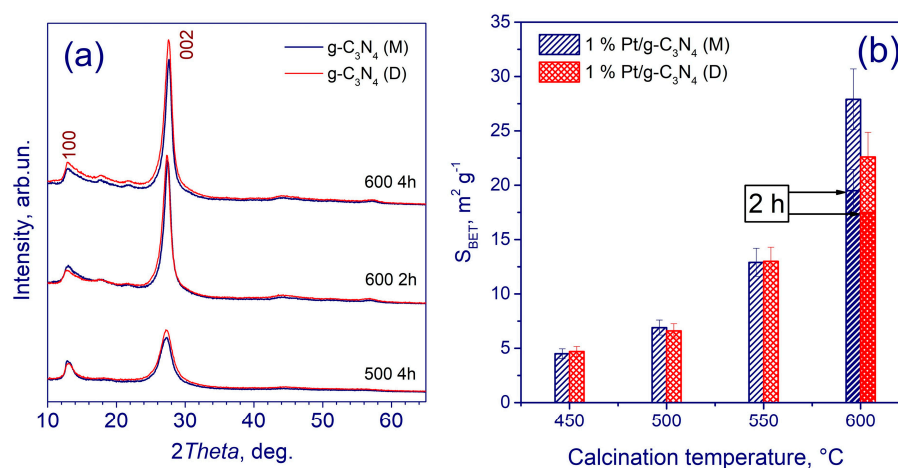


**Figure 3.** (a) XRD patterns of g-C<sub>3</sub>N<sub>4</sub>. (b) Specific surface area photocatalysts obtained from melamine (M) and dicyandiamide (D). Adapted with permission from Ref. [76]. 2021, Elsevier.

The main diffraction peak ( $2\theta \sim 27^\circ$ ) can be assigned to the (002) plane; it determines the distance between the 2D layers of graphitic carbon nitride. The second peak at  $2\theta = 13^\circ$  is due to the distance between tri-s-triazine units (Figure 3a). The specific surface area of photocatalysts increases significantly with an increase in the calcination temperature (Figure 3b). The samples calcined at temperatures of 450 and 500 °C demonstrate low specific surface areas of  $<10 \text{ m}^2 \cdot \text{g}^{-1}$ ; at calcination temperatures of 550 and 600 °C, the

surface increases to  $13\text{--}28\text{ m}^2\cdot\text{g}^{-1}$ . Note that the specific surface area of  $\text{g-C}_3\text{N}_4$  synthesized from melamine exceeds that of  $\text{g-C}_3\text{N}_4$  obtained from dicyandiamide.

Figure 4 illustrates photocatalytic activity of the synthesized samples depending on the calcination conditions.

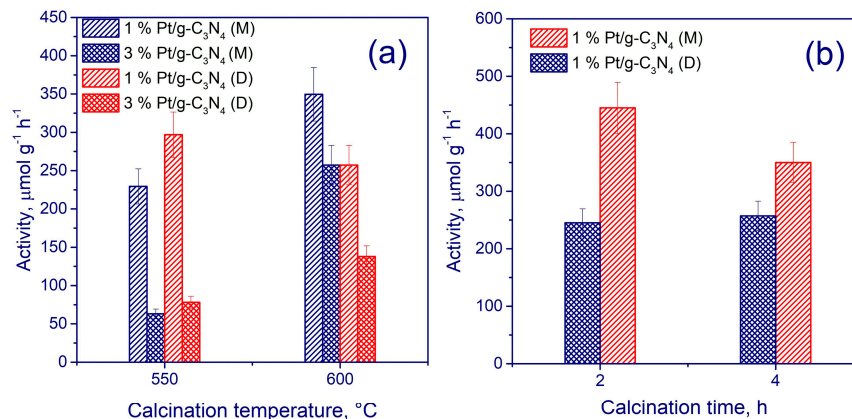


**Figure 4.** (a) Catalytic activity of samples synthesized at 550 and 600 °C for 4 h. (b) Catalytic activity of samples synthesized for 2 and 4 h at 600 °C using photocatalysts obtained from melamine (M) and A dicyandiamide (D). Adapted with permission from Ref. [76]. 2021, Elsevier.

Among a large set of synthesized samples differing by precursors, calcination temperatures (450 to 600 °C) and times (2 or 4 h), the most active photocatalysts were selected (Figure 4). The higher the calcination temperature of the precursors, the more active the photocatalyst, most likely, due to the efficient (more complete) decomposition of melamine and dicyandiamide. Note that the correlation between the catalyst activity and the specific surface area is non-linear. Indeed, the catalyst, synthesized through melamine calcination at 600 °C for 2 h and having a lower specific surface area of  $19.5\text{ m}^2\cdot\text{g}^{-1}$  appeared more active than a similar catalyst calcined for 4 h and having a larger surface area of  $27.9\text{ m}^2\cdot\text{g}^{-1}$ . This observation may be attributed to the optimal interplanar spacing and crystal size in the former sample.

Since platinum facilitates efficient separation of photoinduced charges, it was used as a cocatalyst. The 1 wt. % Pt additive provided a higher catalytic activity than the 3 wt. % one. As a result of the optimization of catalyst preparation procedure, the highest activity for hydrogen production— $0.45\text{ mmol g}_{\text{cat}}^{-1}\cdot\text{h}^{-1}$  (apparent quantum efficiency 0.6%)—showed the 1% Pt/g-C<sub>3</sub>N<sub>4</sub> catalyst synthesized by melamine calcining at 600 °C for 2 h [76].

### 3.2. Synthesis of Graphitic Carbon Nitride from Melamine Hydrothermally Pretreated in Glucose

Based on the above results, melamine was chosen used as the precursor for catalyst synthesis using pretreatment in glucose. Melamine was suspended in an aqueous glucose solution and then heated in an autoclave at 180 °C for 12 h. The resulting material was heated in a furnace to 550 °C at a rate of 1°C/min, kept at this temperature for 1 h and then cooled to room temperature [102]. The synthesized material was used to deposit platinum (0.5 wt %) by various methods [102], one of which—sorption of Pt from nitratocomplex—has already proven itself in the case of deposition on TiO<sub>2</sub> surface [30]. Besides platinum reduction with an excess of sodium borohydride, as described earlier, the following methods were used.

**Photoreduction.** Deaerated suspension consisting of carbon nitride, H<sub>2</sub>PtCl<sub>6</sub>, excess ethanol (20 vol.%) and water was illuminated by LED radiation with a wavelength of 380 nm (30 W).

**Reduction of platinum nitratocomplexes.** Carbon nitride was suspended in acetone and combined with an appropriate aliquot of the (Me<sub>4</sub>N)<sub>2</sub>[Pt<sub>2</sub>(μ-OH)<sub>2</sub>(NO<sub>3</sub>)<sub>8</sub>] acetone solution. The resulting suspension was stirred at room temperature for 12 h, then dried in an air stream. The obtained material was reduced in a hydrogen atmosphere (100–500 °C,

heating rate 10 °C/min) for 1 h. The results of the samples characterization by XRD method proved that they had the structure of graphitic carbon nitride. The samples had the specific surface area ( $S_{\text{BET}}$ ) of  $\sim 25 \text{ m}^2 \cdot \text{g}^{-1}$ , which is quite similar to respective value for the catalysts synthesized through standard procedure with precursor calcination, but the pore system was higher due to the use of glucose.

Obviously, the catalysts reduced by  $\text{NaBH}_4$  contain platinum in states 4+, 2+ and 0, while in photoreduced catalysts, platinum states are 2+ and 0. XPS analysis confirmed that for the samples synthesized with the use of a platinum nitratocomplex and reduced in hydrogen flow at temperatures ranging 100–500 °C, the intensity of peak at 70.7 eV increases with increasing temperature that corresponds to the gradual formation of metallic platinum from adsorbed  $\text{Pt}^{2+}$  species. At 400 °C, platinum is completely reduced to  $\text{Pt}^0$ . Note also that at 500 °C, graphitic carbon nitride is completely destroyed, as proved by further experiments on the samples' photocatalytic activity to produce hydrogen [102].

It has been shown that the sample calcined at 400 °C in  $\text{H}_2$  flow showed the highest catalytic activity (Figure 5a) [102]. The activity of the 0.5%  $\text{Pt}/\text{g-C}_3\text{N}_4$  photocatalysts prepared using platinum nitratocomplexes increases as the temperature of the catalyst reduction in  $\text{H}_2$  elevates to 400 °C and sharply decreases as the temperature reaches 500 °C, because the  $\text{g-C}_3\text{N}_4$  structure is destroyed at this temperature. The kinetic dependences for photocatalytic hydrogen evolution from an aqueous solution of TEOA were also obtained to compare various methods of platinum reduction (Figure 5b).

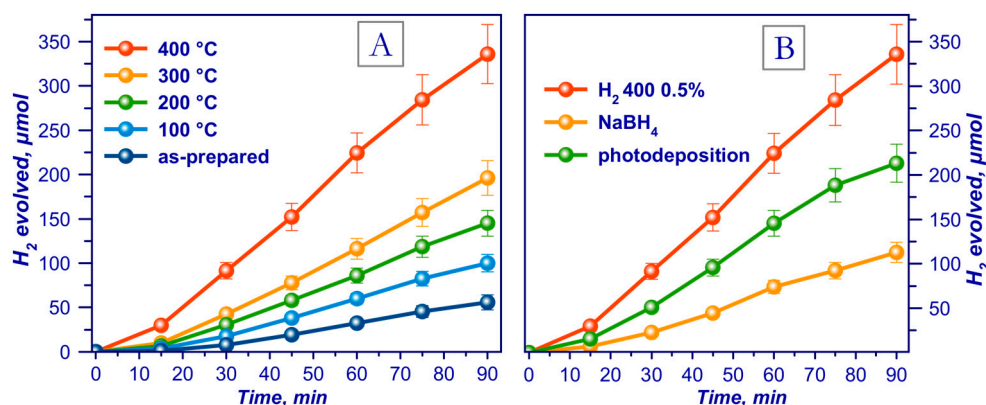


**Figure 5.** Kinetic curves of the photocatalytic evolution of hydrogen from an aqueous solution of triethanolamine (TEOA) over (A) catalysts reduced in  $\text{H}_2$  flow at different temperatures, and (B) using photocatalysts reduced by various methods. Adapted with permission from Ref. [102]. 2022, Elsevier.

It should be noted that the catalyst calcined at 400 °C in hydrogen flow showed the highest activity among all other samples prepared with the proposed methods for platinum deposition and reduction [102].

Furthermore, the photocatalyst demonstrated high stability (Figure 6). After 7.5 h, the rate of photocatalytic hydrogen evolution with this catalyst decreased by only 8%. Note also that hydrogen production rate on this photocatalyst was  $5.3 \text{ mmol g}_{\text{cat}}^{-1} \cdot \text{h}^{-1}$  (apparent quantum efficiency AQE = 3.0% (425 nm)). Thus, as compared to traditional melamine calcination method [76], a 12-fold increase in the catalyst activity and a double reduction in Pt content was achieved.

### 3.3. Synthesis of Graphitic Carbon Nitride from Supramolecular Melamine-Cyanuric Acid Adduct

The next method for the synthesis of graphitic carbon nitride consists in the thermolysis of supramolecular adduct formed by melamine and cyanuric acid [103]. Melamine and cyanuric acid were suspended in distilled water (300 mL); the suspension was heated at 90 °C for 12 h under constant stirring. The resulting material was heated in a furnace to 550 °C at a rate of 1 °C/min and kept at this temperature for 1 h. The obtained  $\text{g-}$

$C_3N_4$  samples were loaded with platinum as described above (reduction of platinum nitratocomplex in hydrogen flow at temperatures 100–400 °C [102]).

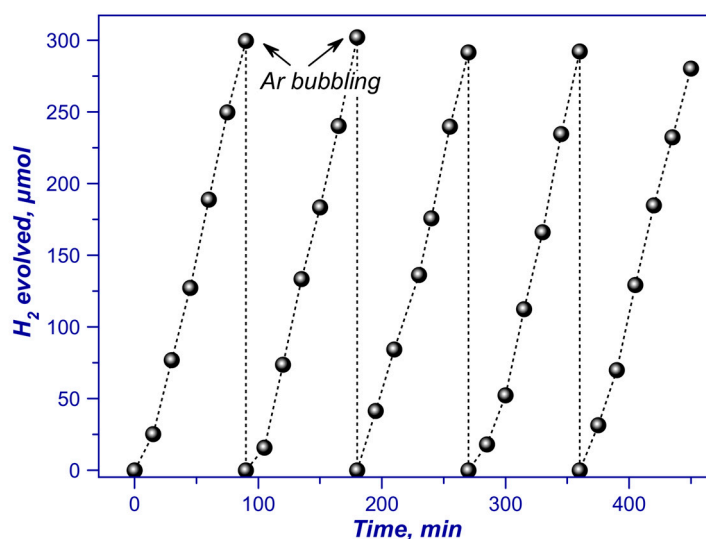


**Figure 6.** Stability of the 0.5% Pt/g- $C_3N_4$  ( $T = 400$  °C) photocatalyst in five 1.5 h cycles of hydrogen production. Adapted with permission from Ref. [102]. 2022, Elsevier.

Graphitic carbon nitride synthesized by this method demonstrated an interesting property – the structural erosion and formation of new pores upon calcination of the samples with adsorbed platinum complexes at a temperature of 400 °C [103]. Thermogravimetric studies in hydrogen atmosphere showed that the decomposition temperature of graphitic carbon nitride synthesized by this method decreases when  $(Me_4N)_2[Pt_2(OH)_2(NO_3)_6]$  complexes are adsorbed on its surface; for 0.5 wt.% Pt/g- $C_3N_4$  this decrease is more significant than for 0.1 wt.% Pt/g- $C_3N_4$ . The decomposition of g- $C_3N_4$  releases ammonia and methane. Note also that the specific surface area of photocatalysts increases with increasing Pt content as well. Indeed, 0.1 wt.% Pt/g- $C_3N_4$  ( $T = 400$  °C) has the specific surface area of  $90\text{ m}^2\cdot\text{g}^{-1}$ ; 0.5 wt.% Pt/g- $C_3N_4$  ( $T = 400$  °C)— $289\text{ m}^2\cdot\text{g}^{-1}$ , while unmodified carrier— $60\text{ m}^2\cdot\text{g}^{-1}$ . Figure 7 illustrates the formation of a developed porous structure upon calcination of the  $(Me_4N)_2[Pt_2(OH)_2(NO_3)_6]/g-C_3N_4(IV)$  samples in hydrogen flow.

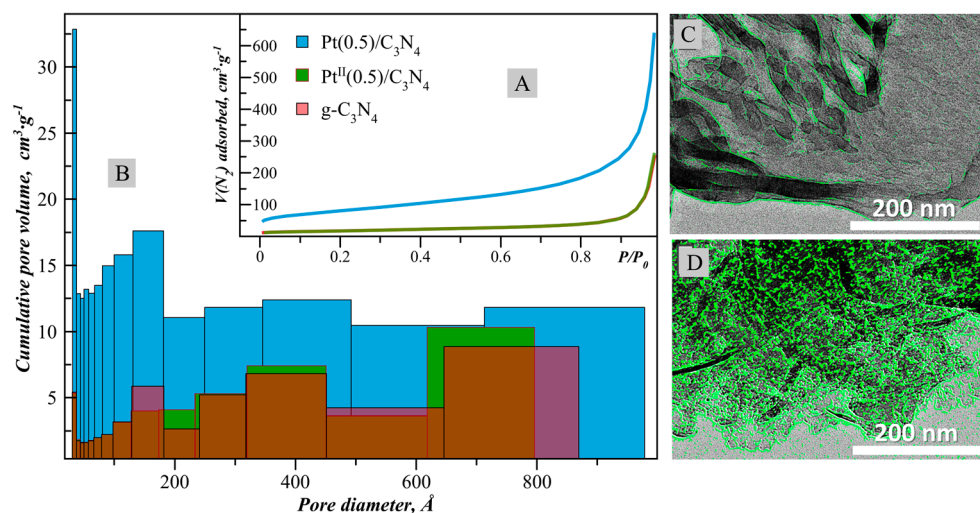


**Figure 7.** (A) Adsorption isotherms; (B) pore size distribution for g- $C_3N_4$ , 0.5% Pt/g- $C_3N_4$  (IV) without treatment and 0.5% Pt/g- $C_3N_4$  (IV) after reduction in  $H_2$  at 400 °C. (C) TEM images of photocatalysts 0.5% Pt/g- $C_3N_4$  (no treatment) and (D) 0.5% Pt/g- $C_3N_4$  ( $T = 400$  °C). Reprinted with permission from Ref. [103]. 2022, Elsevier.

It was shown that the proposed g-C<sub>3</sub>N<sub>4</sub> modifying method, which includes the synthesis of graphitic carbon nitride from the supramolecular melamine-cyanuric acid adduct, the deposition of platinum from the nitratocomplex by sorption method, followed by reduction in H<sub>2</sub> flow at 400 °C, provided photocatalytic hydrogen production under the action of visible light at a rate of 11 mmol g<sub>cat</sub><sup>-1</sup>·h<sup>-1</sup> (apparent quantum efficiency of 6.7%) [103], which exceeds respective values reported in the literature.

Additionally, an interesting dependence was observed for these samples. Catalytic activity per 1 g of Pt noticeably increased with increasing platinum content (0.01, 0.05, and 0.1 wt.% Pt). However, as the mass fraction of Pt increased further from 0.1% to 0.5%, the respective activity value decreased from 8.8 to 2.3 mmol g<sub>Pt</sub><sup>-1</sup>·h<sup>-1</sup>. At the same time, the rate of hydrogen production per 1 g of catalyst for the sample 0.5% Pt/g-C<sub>3</sub>N<sub>4</sub> was about 20% higher than that value for catalyst 0.1% Pt/g-C<sub>3</sub>N<sub>4</sub> (Figure 8a–c). Thus, 0.1 wt.% Pt loading is the optimum for efficient production of hydrogen. The apparent quantum efficiencies of hydrogen production were calculated for different wavelengths (action spectrum) (Figure 8d). The maximum quantum efficiency was 6.6% at a wavelength of 425 nm. The action spectrum of the photocatalyst agrees well with the Kubelka–Munk curve F(R) calculated from the diffuse reflectance spectrum of the 0.5% Pt/g-C<sub>3</sub>N<sub>4</sub> (IV) photocatalyst.

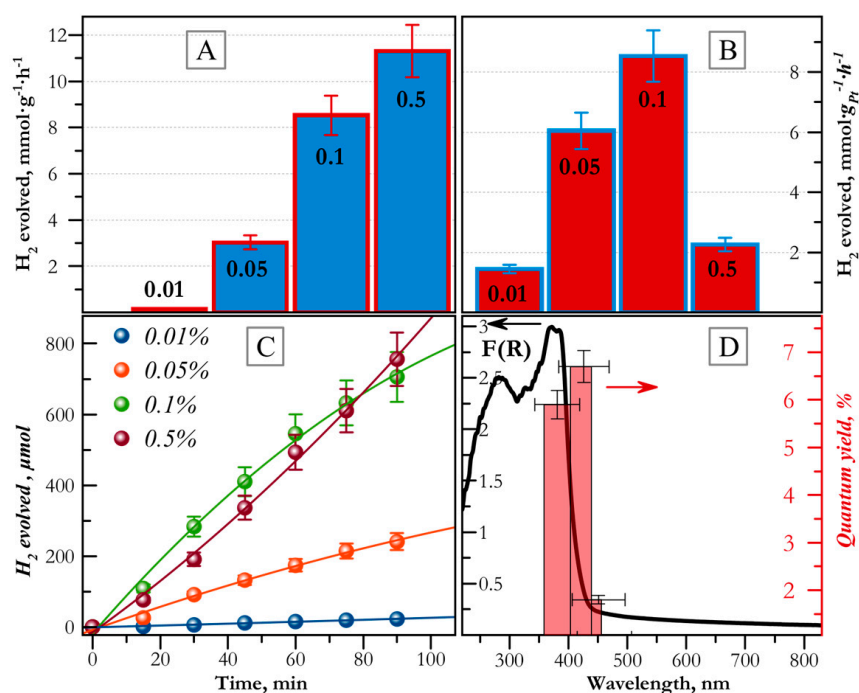


**Figure 8.** Activity of the Pt<sub>x</sub>/g-C<sub>3</sub>N<sub>4</sub> photocatalysts in the reaction of hydrogen evolution ( $\lambda = 425$  nm) calculated by (A) per gram of catalyst; (B) per gram of Pt. (C) Kinetic dependences of the H<sub>2</sub> production reaction under the action of light for Pt<sub>x</sub>/g-C<sub>3</sub>N<sub>4</sub> catalysts. (D) Dependence of the quantum efficiency on the wavelength for the Pt<sub>0.1</sub>/g-C<sub>3</sub>N<sub>4</sub> catalyst. Adapted with permission from Ref. [103]. 2022, Elsevier.

According to the data of the catalyst characterization by physicochemical methods, the treatment with hydrogen of (Me<sub>4</sub>N)<sub>2</sub>[Pt<sub>2</sub>(OH)<sub>2</sub>(NO)<sub>6</sub>]/g-C<sub>3</sub>N<sub>4</sub> composites results in platinum transition into a metallic state followed by catalytical hydrogenation of the g-C<sub>3</sub>N<sub>4</sub> to form methane and ammonia, resulting in an increase in the g-C<sub>3</sub>N<sub>4</sub> specific surface area and branching its porous structure. The observed high values of hydrogen production rate are associated with the proposed approach for the synthesis of photocatalysts based on graphitic carbon nitride. Compared to traditional thermal calcination of the precursor, thermolysis of the supramolecular adduct formed by melamine and cyanuric acid facilitates uniform removal of ammonia groups. Subsequent platinum depositing on the material followed by calcination in a hydrogen flow at 400 °C provides both the complete platinum

reduction to a metallic state, and a significant increase in the specific surface area (up to  $289 \text{ m}^2 \cdot \text{g}^{-1}$  in the case of  $0.5\% \text{ Pt/g-C}_3\text{N}_4$ ), because platinum burns off the surface of graphitic carbon nitride, which induces the formation of new pores and porous structure branching. It should be emphasized also, that the proposed method promotes uniform and tight depositing of platinum nanosized ( $\sim 1 \text{ nm}$ ) particles on the  $\text{g-C}_3\text{N}_4$  surface) [103].

### 3.4. Composites Cd-Zn Sulfide Solid Solution/ $\text{g-C}_3\text{N}_4$

To provide efficient charge separation and, as a consequence, an increase in the catalyst activity, two schemes were proposed to synthesize composites based on  $\text{g-C}_3\text{N}_4$ , Pt, and solid solutions of Cd and Zn sulfides. In Scheme 1, Cd and Zn sulfides were deposited on the surface of  $\text{g-C}_3\text{N}_4$  obtained by the traditional calcination of melamine at  $600 \text{ }^\circ\text{C}$  for 2 h followed by platinum depositing through chemical reduction method. In Scheme 2, platinum was deposited first, and then cadmium and zinc sulfides were loaded [104].

It was shown that in the sample  $1\% \text{ Pt}/20\% \text{ Cd}_{0.8}\text{Zn}_{0.2}\text{S}/\text{g-C}_3\text{N}_4$  synthesized according to Scheme 1, small particles of Pt are deposited on the surface of Cd-Zn sulfide solid solutions. In the sample  $20\% \text{ Cd}_{0.8}\text{Zn}_{0.2}\text{S}/1\% \text{ Pt}/\text{g-C}_3\text{N}_4$  synthesized by Scheme 2, large platinum clusters are located at the  $\text{g-C}_3\text{N}_4/\text{Cd}_{1-x}\text{Zn}_x\text{S}$  interface [104].

All samples synthesized by Scheme 2 were more active than those synthesized by Scheme 1 (Figure 9). It is assumed that within the framework of these Schemes, various mechanisms of charge transfer are realized. In samples  $1\% \text{ Pt}/y\% \text{ Cd}_{1-x}\text{Zn}_x\text{S}/\text{g-C}_3\text{N}_4$  (Scheme 1), the migration of holes and electrons proceeds by type II heterojunction mechanism. Upon illumination, electrons migrate from the CB of  $\text{g-C}_3\text{N}_4$  to the CB of  $\text{Cd}_{1-x}\text{Zn}_x\text{S}$ , and then to Pt, where the photocatalytic reduction reaction occurs. In samples  $y\% \text{ Cd}_{1-x}\text{Zn}_x\text{S}/1\% \text{ Pt}/\text{g-C}_3\text{N}_4$  (Scheme 2), the S-scheme heterojunction is probably realized. At the same time, electrons from the  $\text{g-C}_3\text{N}_4$  CB, possessing high reducing ability, and holes from the  $\text{Cd}_{0.8}\text{Zn}_{0.2}\text{S}$  VB, possessing high oxidizing ability, participate in redox reactions on the photocatalyst surface. Catalyst  $20\% \text{ Cd}_{0.8}\text{Zn}_{0.2}\text{S}/1\% \text{ Pt}/\text{g-C}_3\text{N}_4$  demonstrated the highest value of catalytic activity amounting to  $2.52 \text{ mmol g}_{\text{cat}}^{-1} \cdot \text{h}^{-1}$ . Besides, Scheme 2 photocatalysts are more stable than Scheme I photocatalysts [104].

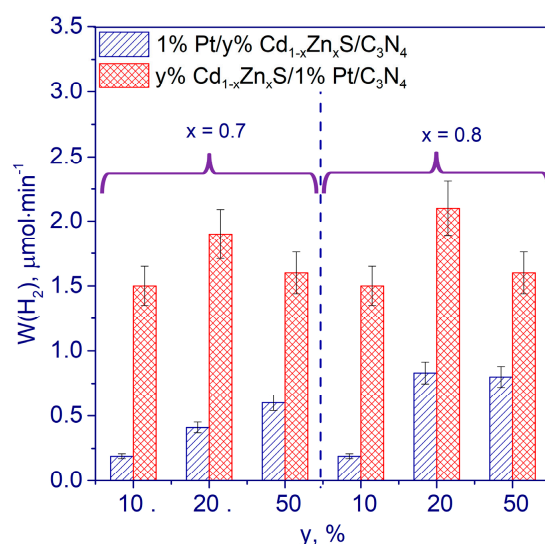


**Figure 9.** Photocatalytic activity of samples  $1\% \text{ Pt}/y\% \text{ Cd}_{1-x}\text{Zn}_x\text{S}/\text{g-C}_3\text{N}_4$  and  $y\% \text{ Cd}_{1-x}\text{Zn}_x\text{S}/1\% \text{ Pt}/\text{g-C}_3\text{N}_4$ . Adapted from [104].

For comparison, the samples containing  $\text{g-C}_3\text{N}_4$  synthesized as described in the above Sections 3.2 and 3.3, and 0.5 wt.% Pt deposited from nitratocomplex, were loaded with 20 wt.% Cd-Zn sulfide solid solution according to Scheme 2. These catalysts appeared more active as compared to those based on  $\text{g-C}_3\text{N}_4$  obtained by the thermal polyconden-

sation of the melamine precursor, and demonstrated hydrogen productivity of 6.3 and 10.2 mmol  $\text{g}_{\text{cat}}^{-1} \cdot \text{h}^{-1}$ , respectively.

### 3.5. Summary Data on the Photocatalysts Based on $g\text{-C}_3\text{N}_4$

Table 1 summarizes the data on the activity of  $g\text{-C}_3\text{N}_4$  based photocatalysts for hydrogen production obtained by the authors of this review. It is seen that the photocatalyst modification with Pt noticeably improved the catalyst activity. The catalyst based on  $g\text{-C}_3\text{N}_4$  synthesized from glucose-pretreated melamine showed a 12-times higher photocatalytic activity in hydrogen production than the sample prepared by the traditional method. The catalyst based on  $g\text{-C}_3\text{N}_4$  synthesized by thermal polycondensation of a supramolecular complex melamine-cyanuric acid, followed by platinum reduction from the nitratocomplex in hydrogen flow at 400 °C, provided a 24-fold increase in the hydrogen production rate as compared to that of the catalyst synthesized through thermal polycondensation of melamine and depositing platinum by the reduction of  $\text{H}_2\text{PtCl}_6$  with  $\text{NaBH}_4$ . It should be emphasized that, besides considerable increase in the catalytic activity, the twice-reduced platinum loading in the catalysts was achieved (0.5 instead of 1 wt.%).

**Table 1.** Comparison of catalytic activities of various photocatalysts described in Chapter 3.

$g\text{-C}_3\text{N}_4$ Synthesis	Pt Deposition			Composites $y\%\text{Cd}_{0.8}\text{Zn}_{0.2}\text{S}/x\%\text{Pt}/g\text{-C}_3\text{N}_4$
	$\text{H}_2\text{PtCl}_6$		$(\text{Me}_4\text{N})_2[\text{Pt}_2(\text{OH})_2(\text{NO}_3)_6]$	
	Reduction by $\text{NaBH}_4$	Photoreduction	$\text{H}_2$ Reduction at 400 °C	
Thermal polycondensation of melamine	0.45	0.87	1.80	2.52
Thermal polycondensation of melamine pretreated in glucose by the hydrothermal method	1.80	4.20	5.30	6.30
Thermal polycondensation of the supramolecular complex melamine-cyanuric acid	3.00	4.90	11.0	10.2

\* All data in the table has a dimension  $\text{mmol g}_{\text{cat}}^{-1} \cdot \text{h}^{-1}$ .

Composite systems based on  $g\text{-C}_3\text{N}_4$ ,  $\text{Cd}_{1-x}\text{Zn}_x\text{S}$ , and Pt were also considered. A significant increase in activity (5.6-fold) showed only the catalyst on the base of  $g\text{-C}_3\text{N}_4$  obtained by thermal polycondensation of melamine. In the case of the other two methods (see Table 1), the increase in activity was either insignificant or not observed at all. This very interesting observation deserves more research and will be explained later.

Table 2 presents the data on catalytic activities in hydrogen production of various photocatalysts based on  $g\text{-C}_3\text{N}_4$  reported in the literature and compares them with the results from Table 1. Clearly, the photocatalyst based on  $g\text{-C}_3\text{N}_4$ , synthesized from the melamine-cyanuric acid supramolecular adduct, with Pt cocatalyst, deposited from Pt-nitratocomplex and reduced in  $\text{H}_2$  at 400 °C, outperforms other catalysts in the photocatalytic production of  $\text{H}_2$ . A comprehensive approach to the synthesis, that provided a high specific surface area of  $g\text{-C}_3\text{N}_4$  and uniform distribution of Pt in the metallic state, allowed the superior catalyst performance in photocatalytic hydrogen production [103]. Also, as another interesting approach, the precipitation of Pt from the acidic solution of platinum hydroxide ( $[\text{Pt}(\text{OH})_4(\text{H}_2\text{O})_2]$ ) has been proposed. This approach is characterized by a simpler method of Pt deposition and is more green, since it does not require the isolation of complex salts and the use of organic solvents in the deposition process [105]. However, the rates of photocatalytic hydrogen production on photocatalysts synthesized by this method were slightly lower than in the case of using the nitratocomplex as a platinum precursor [103].

**Table 2.** Comparison of characteristics of the Pt/g-C<sub>3</sub>N<sub>4</sub> based photocatalysts for hydrogen production reported in the literature and the most active photocatalysts described in Table 1.

Nº	Catalyst	Pt, wt. %	Catalyst Mass, mg	Sacrificial Agent	Synthetic Procedure of Pt	Light Source	H <sub>2</sub> Evolution Rate, $\mu\text{mol min}^{-1}$	Catalytic Activity, $\mu\text{mol g}_{\text{cat}}^{-1}\cdot\text{h}^{-1}$	AQY, %	Ref.
1	0.15-NVCN x—mass KOH heating in N <sub>2</sub> atmosphere	0.5	30	20 vol. % methanol	H <sub>2</sub> PtCl <sub>6</sub> photodeposition in situ	300W Xe lamp $\lambda > 420$ nm	1.66	3310	8.60	[74]
2	g-C <sub>3</sub> N <sub>4</sub>	0.5	10	20 vol. % TEOA	H <sub>2</sub> PtCl <sub>6</sub> Ar plasma	Xe-lamp	0.19	1151	-	[75]
3	g-C <sub>3</sub> N <sub>4</sub> nanosheets	1.25	100	5 vol. % TEOA pH = 9	H <sub>2</sub> PtCl <sub>6</sub> ethylene glycol reduction	300W Xe lamp $\lambda > 420$ nm	0.75	451	-	[106]
4	CNC0.1 0.1%—weight ratio between urea and glucose	1.0	50	15 vol. % TEOA	H <sub>2</sub> PtCl <sub>6</sub> photodeposition in situ	350 W Xe lamp $\lambda \geq 420$ nm	0.18	213	0.90	[107]
5	S-doped g-C <sub>3</sub> N <sub>4</sub> S-CN	0.3	100	15 vol. % methanol	H <sub>2</sub> PtCl <sub>6</sub> photodeposition in situ	300W Xe lamp	1.24	742	-	[108]
6	VCN heating in NH <sub>3</sub> atmosphere	3.0	100	15 vol. % TEOA	H <sub>2</sub> PtCl <sub>6</sub> photodeposition in situ	300W Xe lamp $\lambda > 420$ nm	5.51	3300	-	[109]
7	HCN-3h heating in H <sub>2</sub> atmosphere	3.0	50	15 vol. % TEOA	H <sub>2</sub> PtCl <sub>6</sub> photodeposition in situ	300W Xe lamp	3.58	4300	-	[110]
8	ultrathin O-doped g-C <sub>3</sub> N <sub>4</sub> nanosheets	3.0	5.0	10 vol. % TEOA	H <sub>2</sub> PtCl <sub>6</sub> photodeposition in situ	300W Xe lamp $\lambda > 400$ nm	3.16	3790	-	[111]
9	mesoporous g-C <sub>3</sub> N <sub>4</sub>	0.5	100	10 vol. % iso-propanol	H <sub>2</sub> PtCl <sub>6</sub> photodeposition in situ	medium pressure Hg arc lamp (125W)	3.35	2010	2.72	[112]
10	NiS/g-C <sub>3</sub> N <sub>4</sub> -30 30—time irradiation	-	5	10 vol. % TEOA	-	300W Xe lamp $\lambda > 400$ nm	0.27	3300	1.25	[113]
11	30 wt. % CdS/g-C <sub>3</sub> N <sub>4</sub>	-	20	10 vol. % methanol	-	300W Xe lamp $\lambda > 420$ nm	1.22	3670	2.03	[114]
12	25 wt. % ZnCo <sub>2</sub> S <sub>4</sub> /C <sub>3</sub> N <sub>4</sub>	-	20	20 vol. % TEOA	-	300W Xe lamp $\lambda > 420$ nm	2.21	6620	-	[115]
13	g-C <sub>3</sub> N <sub>4</sub>	0.5	50	10 vol. % TEOA	Reduction of chemisorbed Pt nitrate complex with H <sub>2</sub> at 400 °C	425-nm LED	9.40	11300	6.70	[103]

Table 2. Cont.

No	Catalyst	Pt, wt. %	Catalyst Mass, mg	Sacrificial Agent	Synthetic Procedure of Pt	Light Source	H <sub>2</sub> Evolution Rate, $\mu\text{mol min}^{-1}$	Catalytic Activity, $\mu\text{mol g}_{\text{cat}}^{-1}\cdot\text{h}^{-1}$	AQY, %	Ref.
14	g-C <sub>3</sub> N <sub>4</sub>	0.1	50	10 vol. % TEOA	Reduction of chemisorbed Pt nitrate complex with H <sub>2</sub> at 400 °C	425-nm LED	7.10	8500	5.01	[103]
15	g-C <sub>3</sub> N <sub>4</sub>	0.5	50	10 vol. % TEOA	Reduction of chemisorbed [Pt(OH) <sub>4</sub> (H <sub>2</sub> O) <sub>2</sub> ] with H <sub>2</sub> at 400 °C	425-nm LED	7.10	8500	5.01	[105]

#### 4. Conclusions

Over the past decade, graphitic carbon nitride has been recognized as a promising photocatalytic material and studied in sufficient detail. A lot of approaches to modify graphitic carbon nitride were suggested; the most commonly used methods are described in this review. Analysis of up-to-day research data on this material proved that high rates of hydrogen evolution can be achieved by modifying the textural and electronic characteristics of graphitic carbon nitride. The most promising approaches to solve this task include increasing the specific surface area, creating a branched pore system, and depositing the platinum group metals by various methods.

The authors of the review performed extensive research and proposed various approaches to the synthesis of graphitic carbon nitride, including traditional thermal polycondensation by melamine/dicyandiamide calcination, thermal polycondensation of melamine pretreated hydrothermally with glucose, and thermal polycondensation of the supramolecular melamine-cyanuric acid adduct. Additionally, various methods for depositing the platinum co-catalyst have been suggested. Platinum was deposited from H<sub>2</sub>PtCl<sub>6</sub> and platinum nitratocomplexes and subsequently reduced by various methods, namely, by adding NaBH<sub>4</sub>, photoreduction, or in H<sub>2</sub> flow. It was shown that the best method is to obtain graphitic carbon nitride from the supramolecular melamine-cyanuric acid complex in combination with the platinum depositing from Pt nitratocomplex by sorption method followed by reduction in H<sub>2</sub> flow. This approach allowed the reaching a 11 mmol g<sub>cat</sub><sup>-1</sup>·h<sup>-1</sup> catalytic activity in hydrogen evolution, that significantly exceeds that value of photocatalysts obtained with the use of other combinations of g-C<sub>3</sub>N<sub>4</sub> syntheses and platinum deposition methods. Currently, the proposed materials possess one of the highest performances in photocatalytic production of H<sub>2</sub> as compared to recently published data.

In general, high values of photocatalytic activity of g-C<sub>3</sub>N<sub>4</sub> based systems proposed by the authors of this review, and in other studies considered in the review, show obvious promises for up-scaling the process of photocatalytic hydrogen production towards practically and commercially valid level. However, to move to this level, it is necessary to solve not only the synthesis of active materials, but, for example, the simplification of the synthesis process, the use of environmentally friendly solvents, and the reduction of the content of noble metals in photocatalysts for hydrogen production, which was clearly shown in this study.

**Author Contributions:** Investigation, data curation, visualization, writing—original draft preparation, A.V.Z.; investigation, data curation, visualization, writing—original draft preparation, supervision, conceptualization, D.B.V.; writing—original draft preparation, supervision, conceptualization, funding acquisition, project administration, E.A.K. All authors have read and agreed to the published version of the manuscript.

**Funding:** This work was funded by the Russian Science Foundation (Grant #21-13-00314; <https://rscf.ru/en/project/21-13-00314/>).

**Institutional Review Board Statement:** Not applicable.

**Informed Consent Statement:** Not applicable.

**Data Availability Statement:** The data presented in this study are available on request from the corresponding author.

**Conflicts of Interest:** The authors declare no conflict of interest.

## References

1. Krausmann, F.; Schaffartzik, A.; Mayer, A.; Eisenmenger, N.; Gingrich, S.; Haberl, H.; Fischer-Kowalski, M. Long-Term Trends in Global Material and Energy Use. In *Social Ecology Human-Environment Interactions*; Haberl, H., Fischer-Kowalski, M., Krausmann, F., Winiwarter, V., Eds.; Springer: Cham, Switzerland, 2016; Volume 5, pp. 199–216. [\[CrossRef\]](#)
2. Romanello, M.; Di Napoli, C.; Drummond, P.; Green, C.; Kennard, H.; Lampard, P.; Scamman, D.; Arnell, N.; Ayeb-Karlsson, S.; Ford, L.B.; et al. The 2022 Report of the Lancet Countdown on Health and Climate Change: Health at the Mercy of Fossil Fuels. *Lancet* **2022**, *400*, 1619–1654. [\[CrossRef\]](#) [\[PubMed\]](#)
3. Zhang, B.; Zhang, S.X.; Yao, R.; Wu, Y.H.; Qiu, J.S. Progress and Prospects of Hydrogen Production: Opportunities and Challenges. *J. Electron. Sci. Technol.* **2021**, *19*, 100080. [\[CrossRef\]](#)
4. Aziz, M.; Darmawan, A.; Juangsa, F.B. Hydrogen Production from Biomasses and Wastes: A Technological Review. *Int. J. Hydrogen Energy* **2021**, *46*, 33756–33781. [\[CrossRef\]](#)
5. Sazali, N. Emerging Technologies by Hydrogen: A Review. *Int. J. Hydrogen Energy* **2020**, *45*, 18753–18771. [\[CrossRef\]](#)
6. Zou, C.; Li, J.; Zhang, X.; Jin, X.; Xiong, B.; Yu, H.; Liu, X.; Wang, S.; Li, Y.; Zhang, L.; et al. Industrial Status, Technological Progress, Challenges, and Prospects of Hydrogen Energy. *Nat. Gas Ind. B* **2022**, *9*, 427–447. [\[CrossRef\]](#)
7. Bie, C.; Cheng, B.; Fan, J.; Ho, W.; Yu, J. Enhanced Solar-to-Chemical Energy Conversion of Graphitic Carbon Nitride by Two-Dimensional Cocatalysts. *EnergyChem* **2021**, *3*, 100051. [\[CrossRef\]](#)
8. Ning, X.; Lu, G. Photocorrosion Inhibition of CdS-Based Catalysts for Photocatalytic Overall Water Splitting. *Nanoscale* **2020**, *12*, 1213–1223. [\[CrossRef\]](#)
9. Li, X.; Shen, R.; Ma, S.; Chen, X.; Xie, J. Graphene-Based Heterojunction Photocatalysts. *Appl. Surf. Sci.* **2018**, *430*, 53–107. [\[CrossRef\]](#)
10. Tang, S.; Xia, Y.; Fan, J.; Cheng, B.; Yu, J.; Ho, W. Enhanced Photocatalytic H<sub>2</sub> Production Performance of CdS Hollow Spheres Using C and Pt as Bi-Cocatalysts. *Chin. J. Catal.* **2021**, *42*, 743–752. [\[CrossRef\]](#)
11. Khan, M.; Assal, M.E.; Nawaz Tahir, M.; Khan, M.; Ashraf, M.; Rafe Hatshan, M.; Khan, M.; Varala, R.; Mohammed Badawi, N.; Farooq Adil, S. Graphene/Inorganic Nanocomposites: Evolving Photocatalysts for Solar Energy Conversion for Environmental Remediation. *J. Saudi Chem. Soc.* **2022**, *26*, 101544. [\[CrossRef\]](#)
12. Huang, C.W.; Nguyen, B.S.; Wu, J.C.S.; Nguyen, V.H. A Current Perspective for Photocatalysis towards the Hydrogen Production from Biomass-Derived Organic Substances and Water. *Int. J. Hydrogen Energy* **2020**, *45*, 18144–18159. [\[CrossRef\]](#)
13. Gao, W.; Zhang, S.; Wang, G.; Cui, J.; Lu, Y.; Rong, X.; Gao, C. A Review on Mechanism, Applications and Influencing Factors of Carbon Quantum Dots Based Photocatalysis. *Ceram. Int.* **2022**, *48*, 35986–35999. [\[CrossRef\]](#)
14. Li, X.; Dong, Q.; Tian, Q.; Sial, A.; Wang, H.; Wen, H.; Pan, B.; Zhang, K.; Qin, J.; Wang, C. Recent Advance in Metal- and Covalent-Organic Framework-Based Photocatalysis for Hydrogen Evolution. *Mater. Today Chem.* **2022**, *26*, 101037. [\[CrossRef\]](#)
15. Li, Z.; Li, K.; Du, P.; Mehmandoust, M.; Karimi, F.; Erk, N. Carbon-Based Photocatalysts for Hydrogen Production: A Review. *Chemosphere* **2022**, *308*, 135998. [\[CrossRef\]](#) [\[PubMed\]](#)
16. Durmus, Z.; Maijenburg, A.W. A Review on Graphitic Carbon Nitride (g-C<sub>3</sub>N<sub>4</sub>)—Metal Organic Framework (MOF) Heterostructured Photocatalyst Materials for Photo(Electro)Chemical Hydrogen Evolution. *Int. J. Hydrogen Energy* **2022**, *47*, 36784–36813. [\[CrossRef\]](#)
17. Fujishima, A.; Honda, K. Electrochemical Photolysis of Water at a Semiconductor Electrode. *Nature* **1972**, *238*, 37–38. [\[CrossRef\]](#)
18. Kausar, F.; Varghese, A.; Pinheiro, D.; Devi, K.R.S. Recent Trends in Photocatalytic Water Splitting Using Titania Based Ternary Photocatalysts—A Review. *Int. J. Hydrogen Energy* **2022**, *47*, 22371–22402. [\[CrossRef\]](#)
19. Pattanayak, P.; Singh, P.; Bansal, N.K.; Paul, M.; Dixit, H.; Porwal, S.; Mishra, S.; Singh, T. Recent Progress in Perovskite Transition Metal Oxide-Based Photocatalyst and Photoelectrode Materials for Solar-Driven Water Splitting. *J. Environ. Chem. Eng.* **2022**, *10*, 108429. [\[CrossRef\]](#)
20. Chen, J.; Abazari, R.; Adegoke, K.A.; Maxakato, N.W.; Bello, O.S.; Tahir, M.; Tasleem, S.; Sanati, S.; Kirillov, A.M.; Zhou, Y. Metal–Organic Frameworks and Derived Materials as Photocatalysts for Water Splitting and Carbon Dioxide Reduction. *Coord. Chem. Rev.* **2022**, *469*, 214664. [\[CrossRef\]](#)
21. Hota, P.; Das, A.; Maiti, D.K. A Short Review on Generation of Green Fuel Hydrogen through Water Splitting. *Int. J. Hydrogen Energy* **2022**, in press. [\[CrossRef\]](#)
22. Jaryal, R.; Kumar, R.; Khullar, S. Mixed Metal-Metal Organic Frameworks (MM-MOFs) and Their Use as Efficient Photocatalysts for Hydrogen Evolution from Water Splitting Reactions. *Coord. Chem. Rev.* **2022**, *464*, 214542. [\[CrossRef\]](#)

23. Melián, E.P.; Díaz, O.G.; Méndez, A.O.; López, C.R.; Suárez, M.N.; Rodríguez, J.M.D.; Navío, J.A.; Hevia, D.F.; Peña, J.P. Efficient and Affordable Hydrogen Production by Water Photo-Splitting Using TiO<sub>2</sub>-Based Photocatalysts. *Int. J. Hydrogen Energy* **2013**, *38*, 2144–2155. [[CrossRef](#)]
24. Perumal, V.; Uthrakumar, R.; Chinnathambi, M.; Inmozhi, C.; Robert, R.; Rajasaravanan, M.E.; Raja, A.; Kaviyarasu, K. Electron-Hole Recombination Effect of SnO<sub>2</sub>-CuO Nanocomposite for Improving Methylene Blue Photocatalytic Activity in Wastewater Treatment under Visible Light. *J. King Saud Univ.-Sci.* **2023**, *35*, 102388. [[CrossRef](#)]
25. Meenakshi, G.; Sivasamy, A. Enhanced Photocatalytic Activities of CeO<sub>2</sub>@ZnO Core-Shell Nanostar Particles through Delayed Electron Hole Recombination Process. *Colloids Surfaces A Physicochem. Eng. Asp.* **2022**, *645*, 128920. [[CrossRef](#)]
26. Deng, H.; Qin, C.; Pei, K.; Wu, G.; Wang, M.; Ni, H.; Ye, P. TiO<sub>2</sub>/Reduced Hydroxylated Graphene Nanocomposite Photocatalysts: Improved Electron–Hole Separation and Migration. *Mater. Chem. Phys.* **2021**, *270*, 124796. [[CrossRef](#)]
27. Rozman, N.; Nadrah, P.; Cornut, R.; Joussetme, B.; Bele, M.; Dražić, G.; Gaberšček, M.; Kunej, Š.; Škapin, A.S. TiO<sub>2</sub> Photocatalyst with Single and Dual Noble Metal Co-Catalysts for Efficient Water Splitting and Organic Compound Removal. *Int. J. Hydrogen Energy* **2021**, *46*, 32871–32881. [[CrossRef](#)]
28. Berdyugin, S.; Kozlova, E.; Kurenkova, A.; Gerasimov, E.; Bukhtiyarov, A.; Kolesov, B.; Yushina, I.; Vasilchenko, D.; Korenev, S. Hydrogarnet-Derived Rh/TiO<sub>2</sub> Catalysts with a Low Rhodium Content for a Photocatalytic Hydrogen Production. *Mater. Lett.* **2022**, *307*, 130997. [[CrossRef](#)]
29. Kurenkova, A.Y.; Kremneva, A.M.; Saraev, A.A.; Murzin, V.; Kozlova, E.A.; Kaichev, V.V. Influence of Thermal Activation of Titania on Photoreactivity of Pt/TiO<sub>2</sub> in Hydrogen Production. *Catal. Lett.* **2021**, *151*, 748–754. [[CrossRef](#)]
30. Vasilchenko, D.; Topchian, P.; Tsygankova, A.; Asanova, T.; Kolesov, B.; Bukhtiyarov, A.; Kurenkova, A.; Kozlova, E. Photoinduced Deposition of Platinum from (Bu<sub>4</sub>N)<sub>2</sub>[Pt(NO<sub>3</sub>)<sub>6</sub>] for a Low Pt-Loading Pt/TiO<sub>2</sub> Hydrogen Photogeneration Catalyst. *ACS Appl. Mater. Interfaces* **2020**, *12*, 48631–48641. [[CrossRef](#)]
31. Popugaeva, D.; Tian, T.; Ray, A.K. Hydrogen Production from Aqueous Triethanolamine Solution Using Eosin Y-Sensitized ZnO Photocatalyst Doped with Platinum. *Int. J. Hydrogen Energy* **2020**, *45*, 11097–11107. [[CrossRef](#)]
32. Hitam, C.N.C.; Jalil, A.A. A Review on Exploration of Fe<sub>2</sub>O<sub>3</sub> Photocatalyst towards Degradation of Dyes and Organic Contaminants. *J. Environ. Manag.* **2020**, *258*, 110050. [[CrossRef](#)]
33. Kurenkova, A.Y.; Markovskaya, D.V.; Gerasimov, E.Y.; Prosvirin, I.P.; Cherepanova, S.V.; Kozlova, E.A. New Insights into the Mechanism of Photocatalytic Hydrogen Evolution from Aqueous Solutions of Saccharides over CdS-Based Photocatalysts under Visible Light. *Int. J. Hydrogen Energy* **2020**, *45*, 30165–30177. [[CrossRef](#)]
34. Kozlova, E.A.; Lyulyukin, M.N.; Markovskaya, D.V.; Selishchev, D.S.; Cherepanova, S.V.; Kozlov, D.V. Synthesis of Cd<sub>1-x</sub>Zn<sub>x</sub>S Photocatalysts for Gas-Phase CO<sub>2</sub> Reduction under Visible Light. *Photochem. Photobiol. Sci.* **2019**, *18*, 871–877. [[CrossRef](#)]
35. Liu, X.; Sayed, M.; Bie, C.; Cheng, B.; Hu, B.; Yu, J.; Zhang, L. Hollow CdS-Based Photocatalysts. *J. Mater.* **2021**, *7*, 419–439. [[CrossRef](#)]
36. Palaniswamy, V.K.; Ramasamy, B.; Manoharan, K.; Raman, K.; Sundaram, R. Enhanced Photocatalytic Degradation of Tetracycline Antibiotic Using M-BiVO<sub>4</sub> Photocatalyst under Visible Light Irradiation. *Chem. Phys. Lett.* **2021**, *771*, 138531. [[CrossRef](#)]
37. Gurylev, V. A Review on the Development and Advancement of Ta<sub>2</sub>O<sub>5</sub> as a Promising Photocatalyst. *Mater. Today Sustain.* **2022**, *18*, 100131. [[CrossRef](#)]
38. Lian, J.; Li, D.; Qi, Y.; Yang, N.; Zhang, R.; Xie, T.; Guan, N.; Li, L.; Zhang, F. Metal-Seed Assistant Photodeposition of Platinum over Ta<sub>3</sub>N<sub>5</sub> Photocatalyst for Promoted Solar Hydrogen Production under Visible Light. *J. Energy Chem.* **2021**, *55*, 444–448. [[CrossRef](#)]
39. Hara, M.; Takata, T.; Kondo, J.N.; Domen, K. Photocatalytic Reduction of Water by TaON under Visible Light Irradiation. *Catal. Today* **2004**, *90*, 313–317. [[CrossRef](#)]
40. Ismael, M. Latest Progress on the Key Operating Parameters Affecting the Photocatalytic Activity of TiO<sub>2</sub>-Based Photocatalysts for Hydrogen Fuel Production: A Comprehensive Review. *Fuel* **2021**, *303*, 121207. [[CrossRef](#)]
41. Arora, I.; Chawla, H.; Chandra, A.; Sagadevan, S.; Garg, S. Advances in the Strategies for Enhancing the Photocatalytic Activity of TiO<sub>2</sub>: Conversion from UV-Light Active to Visible-Light Active Photocatalyst. *Inorg. Chem. Commun.* **2022**, *143*, 109700. [[CrossRef](#)]
42. Firtina-Ertis, I.; Kerkez-Kuyumcu, Ö. Synthesis of NiFe<sub>2</sub>O<sub>4</sub>/TiO<sub>2</sub>-Ag<sup>+</sup> S-Scheme Photocatalysts by a Novel Complex-Assisted Vapor Thermal Method for Photocatalytic Hydrogen Production. *J. Photochem. Photobiol. A Chem.* **2022**, *432*, 114106. [[CrossRef](#)]
43. Gao, R.H.; Ge, Q.; Jiang, N.; Cong, H.; Liu, M.; Zhang, Y.Q. Graphitic Carbon Nitride (g-C<sub>3</sub>N<sub>4</sub>)-Based Photocatalytic Materials for Hydrogen Evolution. *Front. Chem.* **2022**, *10*, 1048504. [[CrossRef](#)] [[PubMed](#)]
44. Cao, S.; Yu, J. G-C<sub>3</sub>N<sub>4</sub>-Based Photocatalysts for Hydrogen Generation. *J. Phys. Chem. Lett.* **2014**, *5*, 2101–2107. [[CrossRef](#)] [[PubMed](#)]
45. Alaghmandfard, A.; Ghandi, K. A Comprehensive Review of Graphitic Carbon Nitride (g-C<sub>3</sub>N<sub>4</sub>)-Metal Oxide-Based Nanocomposites: Potential for Photocatalysis and Sensing. *Nanomaterials* **2022**, *12*, 294. [[CrossRef](#)]
46. Xia, P.; Li, G.; Li, X.; Yuan, S.; Wang, K.; Huang, D.; Ji, Y.; Dong, Y.; Wu, X.; Zhu, L.; et al. Synthesis of G-C<sub>3</sub>N<sub>4</sub> from Various Precursors for Photocatalytic H<sub>2</sub> Evolution under the Visible Light. *Crystals* **2022**, *12*, 1719. [[CrossRef](#)]
47. Wang, X.; Maeda, K.; Thomas, A.; Takanabe, K.; Xin, G.; Carlsson, J.M.; Domen, K.; Antonietti, M. A Metal-Free Polymeric Photocatalyst for Hydrogen Production from Water under Visible Light. *Nat. Mater.* **2009**, *8*, 76–80. [[CrossRef](#)]
48. Pati, S.; Acharya, R. An Overview on G-C<sub>3</sub>N<sub>4</sub> as a Robust Photocatalyst towards the Sustainable Generation of H<sub>2</sub> energy. *Mater. Today Proc.* **2021**, *35*, 175–178. [[CrossRef](#)]

49. Mishra, A.; Mehta, A.; Basu, S.; Shetti, N.P.; Reddy, K.R.; Aminabhavi, T.M. Graphitic Carbon Nitride (g-C<sub>3</sub>N<sub>4</sub>)-Based Metal-Free Photocatalysts for Water Splitting: A Review. *Carbon* **2019**, *149*, 693–721. [[CrossRef](#)]
50. Hu, C.; Chiu, W.L.; Wang, C.Y.; Nguyen, V.H. Freeze-Dried Dicyandiamide-Derived g-C<sub>3</sub>N<sub>4</sub> as an Effective Photocatalyst for H<sub>2</sub> Generation. *J. Taiwan Inst. Chem. Eng.* **2021**, *129*, 128–134. [[CrossRef](#)]
51. Liang, L.; Cong, Y.; Wang, F.; Yao, L.; Shi, L. Hydrothermal Pre-Treatment Induced Cyanamide to Prepare Porous g-C<sub>3</sub>N<sub>4</sub> with Boosted Photocatalytic Performance. *Diam. Relat. Mater.* **2019**, *98*, 107499. [[CrossRef](#)]
52. Ong, W.-J.; Tan, L.-L.; Ng, Y.H.; Yong, S.-T.; Chai, S.-P. Graphitic Carbon Nitride (g-C<sub>3</sub>N<sub>4</sub>)-Based Photocatalysts for Artificial Photosynthesis and Environmental Remediation: Are We a Step Closer to Achieving Sustainability? *Chem. Rev.* **2016**, *116*, 7159–7329. [[CrossRef](#)] [[PubMed](#)]
53. Inagaki, M.; Tsumura, T.; Kinumoto, T.; Toyoda, M. Graphitic Carbon Nitrides (g-C<sub>3</sub>N<sub>4</sub>) with Comparative Discussion to Carbon Materials. *Carbon* **2019**, *141*, 580–607. [[CrossRef](#)]
54. Wang, Y.; He, F.; Chen, L.; Shang, J.; Wang, J.; Wang, S.; Song, H.; Zhang, J.; Zhao, C.; Wang, S.; et al. Acidification and Bubble Template Derived Porous G-C<sub>3</sub>N<sub>4</sub> for Efficient Photodegradation and Hydrogen Evolution. *Chin. Chem. Lett.* **2020**, *31*, 2668–2672. [[CrossRef](#)]
55. Wu, X.; Ma, H.; Zhong, W.; Fan, J.; Yu, H. Porous Crystalline G-C<sub>3</sub>N<sub>4</sub>: Bifunctional NaHCO<sub>3</sub> Template-Mediated Synthesis and Improved Photocatalytic H<sub>2</sub>-Evolution Rate. *Appl. Catal. B Environ.* **2020**, *271*, 118899. [[CrossRef](#)]
56. Zhang, H.; Bao, C.; Hu, X.; Wen, Y.; Li, K.; Zhang, H. Synthesis of Tunnel Structured G-C<sub>3</sub>N<sub>4</sub> through a Facile Vapor Deposition Method Using SBA-15 and KIT-6 as Templates and Their Photocatalytic Degradation of Tetracycline Hydrochloride and Phenol. *J. Environ. Chem. Eng.* **2022**, *10*, 107871. [[CrossRef](#)]
57. Ramesh, A.; Da, C.T.; Manigandan, R.; Bhargav, P.B.; Nguyen-Le, M.T. Selectivity Oxidation of Benzyl Alcohol Using Mesoporous G-C<sub>3</sub>N<sub>4</sub> Catalysts Prepared by Hard Template Method. *Colloids Interface Sci. Commun.* **2022**, *48*, 100608. [[CrossRef](#)]
58. Iqbal, W.; Wang, L.; Tan, X.; Zhang, J. One-Step in Situ Green Template Mediated Porous Graphitic Carbon Nitride for Efficient Visible Light Photocatalytic Activity. *J. Environ. Chem. Eng.* **2017**, *5*, 3500–3507. [[CrossRef](#)]
59. Sun, S.; Li, J.; Song, P.; Cui, J.; Yang, Q.; Zheng, X.; Yang, Z.; Liang, S. Facile Constructing of Isotype G-C<sub>3</sub>N<sub>4</sub>(Bulk)/g-C<sub>3</sub>N<sub>4</sub>(Nanosheet) Heterojunctions through Thermal Polymerization of Single-Source Glucose-Modified Melamine: An Efficient Charge Separation System for Photocatalytic Hydrogen Production. *Appl. Surf. Sci.* **2020**, *500*, 143985. [[CrossRef](#)]
60. Yang, Z.; Zhang, Y.; Schnepf, Z. Soft and Hard Templating of Graphitic Carbon Nitride. *J. Mater. Chem. A* **2015**, *3*, 14081–14092. [[CrossRef](#)]
61. Wu, X.; Gao, D.; Wang, P.; Yu, H.; Yu, J. NH<sub>4</sub>Cl-Induced Low-Temperature Formation of Nitrogen-Rich g-C<sub>3</sub>N<sub>4</sub> Nanosheets with Improved Photocatalytic Hydrogen Evolution. *Carbon* **2019**, *153*, 757–766. [[CrossRef](#)]
62. Li, R.; Cui, X.; Bi, J.; Ji, X.; Li, X.; Wang, N.; Huang, Y.; Huang, X.; Hao, H. Urea-Induced Supramolecular Self-Assembly Strategy to Synthesize Wrinkled Porous Carbon Nitride Nanosheets for Highly-Efficient Visible-Light Photocatalytic Degradation. *RSC Adv.* **2021**, *11*, 23459–23470. [[CrossRef](#)] [[PubMed](#)]
63. Babu, B.; Shim, J.; Kadam, A.N.; Yoo, K. Modification of Porous G-C<sub>3</sub>N<sub>4</sub> Nanosheets for Enhanced Photocatalytic Activity: In-Situ Synthesis and Optimization of NH<sub>4</sub>Cl Quantity. *Catal. Commun.* **2019**, *124*, 123–127. [[CrossRef](#)]
64. Wang, Y.; Tan, G.; Dang, M.; Dong, S.; Liu, Y.; Liu, T.; Ren, H.; Xia, A.; Lv, L. Study on Surface Modification of G-C<sub>3</sub>N<sub>4</sub> Photocatalyst. *J. Alloys Compd.* **2022**, *908*, 164507. [[CrossRef](#)]
65. Cui, J.; Qi, D.; Wang, X. Research on the Techniques of Ultrasound-Assisted Liquid-Phase Peeling, Thermal Oxidation Peeling and Acid-Base Chemical Peeling for Ultra-Thin Graphite Carbon Nitride Nanosheets. *Ultrason. Sonochem.* **2018**, *48*, 181–187. [[CrossRef](#)] [[PubMed](#)]
66. Ghosh, U.; Pal, A. Drastically Enhanced Tetracycline Degradation Performance of a Porous 2D G-C<sub>3</sub>N<sub>4</sub> Nanosheet Photocatalyst in Real Water Matrix: Influencing Factors and Mechanism Insight. *J. Water Process Eng.* **2022**, *50*, 103315. [[CrossRef](#)]
67. Liu, G.; Niu, P.; Sun, C.; Smith, S.C.; Chen, Z.; Lu, G.Q.; Cheng, H.M. Unique Electronic Structure Induced High Photoreactivity of Sulfur-Doped Graphitic C<sub>3</sub>N<sub>4</sub>. *J. Am. Chem. Soc.* **2010**, *132*, 11642–11648. [[CrossRef](#)] [[PubMed](#)]
68. Zhang, W.; Xu, D.; Wang, F.; Liu, H.; Chen, M. Enhanced Photocatalytic Performance of S/Cd Co-Doped g-C<sub>3</sub>N<sub>4</sub> Nanorods for Degradation of Dyes. *Colloids Surfaces A Physicochem. Eng. Asp.* **2022**, *653*, 130079. [[CrossRef](#)]
69. Chi, X.; Liu, F.; Gao, Y.; Song, J.; Guan, R.; Yuan, H. An Efficient B/Na Co-Doped Porous g-C<sub>3</sub>N<sub>4</sub> Nanosheets Photocatalyst with Enhanced Photocatalytic Hydrogen Evolution and Degradation of Tetracycline under Visible Light. *Appl. Surf. Sci.* **2022**, *576*, 151837. [[CrossRef](#)]
70. Xu, J.; Chen, Y.; Chen, M.; Wang, J.; Wang, L. In Situ Growth Strategy Synthesis of Single-Atom Nickel/Sulfur Co-Doped g-C<sub>3</sub>N<sub>4</sub> for Efficient Photocatalytic Tetracycline Degradation and CO<sub>2</sub> Reduction. *Chem. Eng. J.* **2022**, *442*, 136208. [[CrossRef](#)]
71. Tan, Y.; Chen, W.; Liao, G.; Li, X.; Wang, J.; Tang, Y.; Li, L. Strategy for Improving Photocatalytic Ozonation Activity of G-C<sub>3</sub>N<sub>4</sub> by Halogen Doping for Water Purification. *Appl. Catal. B Environ.* **2022**, *306*, 121133. [[CrossRef](#)]
72. Zhu, B.; Zhang, J.; Jiang, C.; Cheng, B.; Yu, J. First Principle Investigation of Halogen-Doped Monolayer g-C<sub>3</sub>N<sub>4</sub> Photocatalyst. *Appl. Catal. B Environ.* **2017**, *207*, 27–34. [[CrossRef](#)]
73. Guo, P.; Zhao, F.; Hu, X. Boron- and Europium-Co-Doped g-C<sub>3</sub>N<sub>4</sub> Nanosheets: Enhanced Photocatalytic Activity and Reaction Mechanism for Tetracycline Degradation. *Ceram. Int.* **2021**, *47*, 16256–16268. [[CrossRef](#)]
74. Huang, K.; Li, C.; Yang, J.; Zheng, R.; Wang, W.; Wang, L. Platinum Nanodots Modified Nitrogen-Vacancies g-C<sub>3</sub>N<sub>4</sub> Schottky Junction for Enhancing Photocatalytic Hydrogen Evolution. *Appl. Surf. Sci.* **2022**, *581*, 152298. [[CrossRef](#)]

75. Ding, J.; Sun, X.; Wang, Q.; Li, D.S.; Li, X.; Li, X.; Chen, L.; Zhang, X.; Tian, X.; Ostrikov, K. (Ken) Plasma Synthesis of Pt/g-C<sub>3</sub>N<sub>4</sub> Photocatalysts with Enhanced Photocatalytic Hydrogen Generation. *J. Alloys Compd.* **2021**, *873*, 159871. [[CrossRef](#)]
76. Zhurenok, A.V.; Larina, T.V.; Markovskaya, D.V.; Cherepanova, S.V.; Mel'gunova, E.A.; Kozlova, E.A. Synthesis of Graphitic Carbon Nitride-Based Photocatalysts for Hydrogen Evolution under Visible Light. *Mendeleev Commun.* **2021**, *31*, 157–159. [[CrossRef](#)]
77. Qin, Y.; Lu, J.; Meng, F.; Lin, X.; Feng, Y.; Yan, Y.; Meng, M. Rationally Constructing of a Novel 2D/2D WO<sub>3</sub>/Pt/g-C<sub>3</sub>N<sub>4</sub> Schottky-Ohmic Junction towards Efficient Visible-Light-Driven Photocatalytic Hydrogen Evolution and Mechanism Insight. *J. Colloid Interface Sci.* **2021**, *586*, 576–587. [[CrossRef](#)]
78. Zhao, G.; Huang, X.; Fina, F.; Zhang, G.; Irvine, J.T.S. Facile Structure Design Based on C<sub>3</sub>N<sub>4</sub> for Mediator-Free Z-Scheme Water Splitting under Visible Light. *Catal. Sci. Technol.* **2015**, *5*, 3416–3422. [[CrossRef](#)]
79. Han, C.; Du, L.; Konarova, M.; Qi, D.-C.; Phillips, D.L.; Xu, J. Beyond Hydrogen Evolution: Solar-Driven, Water-Donating Transfer Hydrogenation over Platinum/Carbon Nitride. *ACS Catal.* **2020**, *10*, 9227–9235. [[CrossRef](#)]
80. Wang, L.; Zang, L.; Shen, F.; Wang, J.; Yang, Z.; Zhang, Y.; Sun, L. Preparation of Cu Modified G-C<sub>3</sub>N<sub>4</sub> Nanorod Bundles for Efficiently Photocatalytic CO<sub>2</sub> Reduction. *J. Colloid Interface Sci.* **2022**, *622*, 336–346. [[CrossRef](#)]
81. Bi, L.; Xu, D.; Zhang, L.; Lin, Y.; Wang, D.; Xie, T. Metal Ni-Loaded g-C<sub>3</sub>N<sub>4</sub> for Enhanced Photocatalytic H<sub>2</sub> Evolution Activity: The Change in Surface Band Bending. *Phys. Chem. Chem. Phys.* **2015**, *17*, 29899–29905. [[CrossRef](#)]
82. Zhou, X.; Wang, Y.; Wang, Y.; Zhang, M.; Gao, H.; Zhang, X. Superior Uniform Carbon Nanofibers@g-C<sub>3</sub>N<sub>4</sub> Core-Shell Nanostructures Embedded by Au Nanoparticles for High-Efficiency Photocatalyst. *J. Hazard. Mater.* **2020**, *388*, 121759. [[CrossRef](#)] [[PubMed](#)]
83. Shiraishi, Y.; Kofuji, Y.; Kanazawa, S.; Sakamoto, H.; Ichikawa, S.; Tanaka, S.; Hirai, T. Platinum Nanoparticles Strongly Associated with Graphitic Carbon Nitride as Efficient Co-Catalysts for Photocatalytic Hydrogen Evolution under Visible Light. *Chem. Commun.* **2014**, *50*, 15255–15258. [[CrossRef](#)] [[PubMed](#)]
84. Liu, D.; Shen, J.; Xie, Y.; Qiu, C.; Zhang, Z.; Long, J.; Lin, H.; Wang, X. Metallic Pt and PtO<sub>2</sub> Dual-Cocatalyst-Loaded Binary Composite RGO-CN<sub>x</sub> for the Photocatalytic Production of Hydrogen and Hydrogen Peroxide. *ACS Sustain. Chem. Eng.* **2021**, *9*, 6380–6389. [[CrossRef](#)]
85. Guo, Y.; Jia, H.; Yang, J.; Yin, H.; Yang, Z.; Wang, J.; Yang, B. Understanding the Roles of Plasmonic Au Nanocrystal Size, Shape, Aspect Ratio and Loading Amount in Au/g-C<sub>3</sub>N<sub>4</sub> Hybrid Nanostructures for Photocatalytic Hydrogen Generation. *Phys. Chem. Chem. Phys.* **2018**, *20*, 22296–22307. [[CrossRef](#)] [[PubMed](#)]
86. Li, L.; Wang, X.; Gu, H.; Zhang, H.; Zhang, J.; Zhang, Q.; Dai, W.L. Which Is More Efficient in Promoting the Photocatalytic H<sub>2</sub> Evolution Performance of G-C<sub>3</sub>N<sub>4</sub>: Monometallic Nanocrystal, Heterostructural Nanocrystal, or Bimetallic Nanocrystal? *Inorg. Chem.* **2022**, *61*, 4760–4768. [[CrossRef](#)] [[PubMed](#)]
87. Fei, H.; Shao, J.; Li, H.; Li, N.; Chen, D.; Xu, Q.; He, J.; Lu, J. Construction of Ultra-Thin 2D CN-Br<sub>0.12</sub>/2%RhO<sub>x</sub> Photo-Catalyst with Rapid Electron and Hole Separation for Efficient Bisphenol A Degradation. *Appl. Catal. B Environ.* **2021**, *299*, 120623. [[CrossRef](#)]
88. Alwin, E.; Wojcieszak, R.; Kočí, K.; Edelmannová, M.; Zieliński, M.; Suchora, A.; Pędziński, T.; Pietrowski, M. Reductive Modification of Carbon Nitride Structure by Metals—The Influence on Structure and Photocatalytic Hydrogen Evolution. *Materials* **2022**, *15*, 710. [[CrossRef](#)]
89. Zhang, L.; Long, R.; Zhang, Y.; Duan, D.; Xiong, Y.; Zhang, Y.; Bi, Y. Direct Observation of Dynamic Bond Evolution in Single-Atom Pt/C<sub>3</sub>N<sub>4</sub> Catalysts. *Angew. Chem.* **2020**, *132*, 6283–6288. [[CrossRef](#)]
90. Li, H.; Zhao, J.; Geng, Y.; Li, Z.; Li, Y.; Wang, J. Construction of CoP/B Doped g-C<sub>3</sub>N<sub>4</sub> Nanodots/g-C<sub>3</sub>N<sub>4</sub> Nanosheets Ternary Catalysts for Enhanced Photocatalytic Hydrogen Production Performance. *Appl. Surf. Sci.* **2019**, *496*, 143738. [[CrossRef](#)]
91. Zhu, Y.; Wan, T.; Wen, X.; Chu, D.; Jiang, Y. Tunable Type I and II Heterojunction of CoO<sub>x</sub> Nanoparticles Confined in G-C<sub>3</sub>N<sub>4</sub> Nanotubes for Photocatalytic Hydrogen Production. *Appl. Catal. B Environ.* **2019**, *244*, 814–822. [[CrossRef](#)]
92. Wang, Y.; Li, J.; Chen, S.; Xie, Y.; Ma, Y.; Luo, Y.; Huang, J.; Ling, Y.; Ye, J.; Liang, Y.; et al. In Situ Loading of ZnIn<sub>2</sub>S<sub>4</sub> Nanosheets onto S Doped G-C<sub>3</sub>N<sub>4</sub> Nanosheets to Construct Type II Heterojunctions for Improving Photocatalytic Hydrogen Production. *J. Alloys Compd.* **2022**, *924*, 166569. [[CrossRef](#)]
93. Van, K.N.; Huu, H.T.; Nguyen Thi, V.N.; Le Thi, T.L.; Truong, D.H.; Truong, T.T.; Dao, N.N.; Vo, V.; Tran, D.L.; Vasseghian, Y. Facile Construction of S-Scheme SnO<sub>2</sub>/g-C<sub>3</sub>N<sub>4</sub> Photocatalyst for Improved Photoactivity. *Chemosphere* **2022**, *289*, 133120. [[CrossRef](#)] [[PubMed](#)]
94. Zhang, T.; Yang, Q.; Li, H.; Zhong, J.; Li, J.; Yang, H. Photocatalytic Properties of BiOBr/g-C<sub>3</sub>N<sub>4</sub> Heterojunctions Originated from S-Scheme Separation and Transfer of Interfacial Charge Pairs. *Opt. Mater.* **2022**, *131*, 112649. [[CrossRef](#)]
95. Ma, Y.; Li, J.; Cai, J.; Zhong, L.; Lang, Y.; Ma, Q. Z-Scheme g-C<sub>3</sub>N<sub>4</sub>/ZnS Heterojunction Photocatalyst: One-Pot Synthesis, Interfacial Structure Regulation, and Improved Photocatalysis Activity for Bisphenol A. *Colloids Surfaces A Physicochem. Eng. Asp.* **2022**, *653*, 130027. [[CrossRef](#)]
96. Bi, Z.; Guo, R.; Ji, X.; Hu, X.; Wang, J.; Chen, X.; Pan, W. Direct Z-Scheme CoS/g-C<sub>3</sub>N<sub>4</sub> Heterojunction with NiS Co-Catalyst for Efficient Photocatalytic Hydrogen Generation. *Int. J. Hydrogen Energy* **2022**, *47*, 34430–34443. [[CrossRef](#)]
97. Qi, K.; Cheng, B.; Yu, J.; Ho, W. A Review on TiO<sub>2</sub>-Based Z-Scheme Photocatalysts. *Cuihua Xuebao/Chin. J. Catal.* **2017**, *38*, 1936–1955. [[CrossRef](#)]

98. Li, Y.; Wang, X.; Huo, H.; Li, Z.; Shi, J. A Novel Binary Visible-Light-Driven Photocatalyst Type-I CdIn<sub>2</sub>S<sub>4</sub>/g-C<sub>3</sub>N<sub>4</sub> Heterojunctions Coupling with H<sub>2</sub>O<sub>2</sub>: Synthesis, Characterization, Photocatalytic Activity for Reactive Blue 19 Degradation and Mechanism Analysis. *Colloids Surfaces A Physicochem. Eng. Asp.* **2020**, *587*, 124322. [[CrossRef](#)]
99. Li, Y.; Zhou, M.; Cheng, B.; Shao, Y. Recent Advances in G-C<sub>3</sub>N<sub>4</sub>-Based Heterojunction Photocatalysts. *J. Mater. Sci. Technol.* **2020**, *56*, 1–17. [[CrossRef](#)]
100. Li, Y.; Xia, Z.; Yang, Q.; Wang, L.; Xing, Y. Review on G-C<sub>3</sub>N<sub>4</sub>-Based S-Scheme Heterojunction Photocatalysts. *J. Mater. Sci. Technol.* **2022**, *125*, 128–144. [[CrossRef](#)]
101. Li, Y.; He, Z.; Liu, L.; Jiang, Y.; Ong, W.J.; Duan, Y.; Ho, W.; Dong, F. Inside-and-out Modification of Graphitic Carbon Nitride (g-C<sub>3</sub>N<sub>4</sub>) Photocatalysts via Defect Engineering for Energy and Environmental Science. *Nano Energy* **2023**, *105*, 108032. [[CrossRef](#)]
102. Vasilchenko, D.; Zhurenok, A.; Saraev, A.; Gerasimov, E.; Cherepanova, S.; Kovtunova, L.; Tkachev, S.; Kozlova, E. Platinum Deposition onto G-C<sub>3</sub>N<sub>4</sub> with Using of Labile Nitratocomplex for Generation of the Highly Active Hydrogen Evolution Photocatalysts. *Int. J. Hydrogen Energy* **2022**, *47*, 11326–11340. [[CrossRef](#)]
103. Vasilchenko, D.; Zhurenok, A.; Saraev, A.; Gerasimov, E.; Cherepanova, S.; Tkachev, S.; Plusnin, P.; Kozlova, E. Highly Efficient Hydrogen Production under Visible Light over G-C<sub>3</sub>N<sub>4</sub>-Based Photocatalysts with Low Platinum Content. *Chem. Eng. J.* **2022**, *445*, 136721. [[CrossRef](#)]
104. Zhurenok, A.V.; Markovskaya, D.V.; Gerasimov, E.Y.; Vokhmintsev, A.S.; Weinstein, I.A.; Prosvirin, I.P.; Cherepanova, S.V.; Bukhtiyarov, A.V.; Kozlova, E.A. Constructing G-C<sub>3</sub>N<sub>4</sub>/Cd<sub>1-x</sub>Zn<sub>x</sub>S-Based Heterostructures for Efficient Hydrogen Production under Visible Light. *Catalysts* **2021**, *11*, 1340. [[CrossRef](#)]
105. Vasilchenko, D.; Tkachenko, P.; Tkachev, S.; Popovetskiy, P.; Komarov, V.; Asanova, T.; Asanov, I.; Filatov, E.; Maximovskiy, E.; Gerasimov, E.; et al. Sulfuric Acid Solutions of [Pt(OH)<sub>4</sub>(H<sub>2</sub>O)<sub>2</sub>]: A Platinum Speciation Survey and Hydrated Pt(IV) Oxide Formation for Practical Use. *Inorg. Chem.* **2022**, *61*, 9667–9684. [[CrossRef](#)]
106. Wang, Y.; Hong, J.; Zhang, W.; Rong, X. Carbon Nitride Nanosheets for Photocatalytic Hydrogen Evolution: Remarkably Enhanced Activity by Dye Sensitization. *Catal. Sci.* **2013**, *3*, 1703–1711. [[CrossRef](#)]
107. Xu, Q.; Cheng, B.; Yu, J.; Liu, G. Making Co-Condensed Amorphous Carbon/g-C<sub>3</sub>N<sub>4</sub> Composites with Improved Visible-Light Photocatalytic H<sub>2</sub>-Production Performance Using Pt as Cocatalyst. *Carbon N. Y.* **2017**, *118*, 241–249. [[CrossRef](#)]
108. Li, Z.; Yao, Y.; Gao, X.; Bai, H.; Meng, X. Interfacial Charge Transfer and Enhanced Photocatalytic Mechanisms for Pt Nanoparticles Loaded onto Sulfur-Doped g-C<sub>3</sub>N<sub>4</sub> in H<sub>2</sub> Evolution. *Mater. Today Energy* **2021**, *22*, 100881. [[CrossRef](#)]
109. Rao, F.; Zhong, J.; Li, J. Improved Visible Light Responsive Photocatalytic Hydrogen Production over G-C<sub>3</sub>N<sub>4</sub> with Rich Carbon Vacancies. *Ceram. Int.* **2022**, *48*, 1439–1445. [[CrossRef](#)]
110. Li, Y.; Zhong, J.; Li, J. Rich Carbon Vacancies Facilitated Solar Light-Driven Photocatalytic Hydrogen Generation over g-C<sub>3</sub>N<sub>4</sub> Treated in H<sub>2</sub> Atmosphere. *Int. J. Hydrogen Energy* **2022**, *47*, 39886–39897. [[CrossRef](#)]
111. She, X.; Liu, L.; Ji, H.; Mo, Z.; Li, Y.; Huang, L.; Du, D.; Xu, H.; Li, H. Template-Free Synthesis of 2D Porous Ultrathin Nonmetal-Doped g-C<sub>3</sub>N<sub>4</sub> Nanosheets with Highly Efficient Photocatalytic H<sub>2</sub> Evolution from Water under Visible Light. *Appl. Catal. B Environ.* **2016**, *187*, 144–153. [[CrossRef](#)]
112. Obregón, S.; Vázquez, A.; Ruíz-Gómez, M.A.; Rodríguez-González, V. SBA-15 Assisted Preparation of Mesoporous g-C<sub>3</sub>N<sub>4</sub> for Photocatalytic H<sub>2</sub> Production and Au<sup>3+</sup> Fluorescence Sensing. *Appl. Surf. Sci.* **2019**, *488*, 205–212. [[CrossRef](#)]
113. Chen, L.; Yang, Z.; Chen, B. Uniformly Dispersed Metal Sulfide Nanodots on G-C<sub>3</sub>N<sub>4</sub> as Bifunctional Catalysts for High-Efficiency Photocatalytic H<sub>2</sub> and H<sub>2</sub>O<sub>2</sub> Production under Visible-Light Irradiation. *Energy Fuels* **2021**, *35*, 10746–10755. [[CrossRef](#)]
114. Fiqar, Z.; Tao, J.; Yang, T.; Liu, Q.; Hu, J.; Tang, H. Designing 0D/2D CdS Nanoparticles/g-C<sub>3</sub>N<sub>4</sub> Nanosheets Heterojunction as Efficient Photocatalyst for Improved H<sub>2</sub>-Evolution. *Surf. Interfaces* **2021**, *26*, 101312. [[CrossRef](#)]
115. Wang, C.; Zhang, W.; Fan, J.; Sun, W.; Liu, E. S-Scheme Bimetallic Sulfide ZnCo<sub>2</sub>S<sub>4</sub>/g-C<sub>3</sub>N<sub>4</sub> Heterojunction for Photocatalytic H<sub>2</sub> Evolution. *Ceram. Int.* **2021**, *47*, 30194–30202. [[CrossRef](#)]

**Disclaimer/Publisher's Note:** The statements, opinions and data contained in all publications are solely those of the individual author(s) and contributor(s) and not of MDPI and/or the editor(s). MDPI and/or the editor(s) disclaim responsibility for any injury to people or property resulting from any ideas, methods, instructions or products referred to in the content.